Research Square

Preprints are preliminary reports that have not undergone peer review.
They should not be considered conclusive, used to inform clinical practice,
or referenced by the media as validated information.

Global Geographic, Seasonal, Environmental and Demographic Drivers of Variations in Longitudinal Cardiac Physiology in 5 million Fitbit Users

Katarina Vukosavljević
Google Research; Institute of Biomedical Engineering, University of Oxford, Oxford, UK
Abram Schönfeldt
Google Research; Nuffield Department of Population Health, University of Oxford, Oxford, UK
Justin Phillips
Google Research, Mountain View, CA, USA
Yongsuk Cho
Google Research, Mountain View, CA, USA
Tingting Zhu
Institute of Biomedical Engineering, University of Oxford, Oxford, UK
Shwetak Patel
Google Research; Paul G. Allen School of Computer Science and Engineering, University of Washington
Soren Brage
IMS Epidemiology, University of Cambridge, School of Clinical Medicine, Cambridge, UK
Robert Harle
Google Research; Department of Computer Science and Technology, University of Cambridge, Cambridge, UK
Daniel Roggen
roggen@google.com

Google Research; School of Engineering & Informatics, University of Sussex, UK

Article

Keywords:

Posted Date: September 14th, 2026

DOI: https://doi.org/10.21203/rs.3.rs-10785318/v1

License: This work is licensed under a Creative Commons Attribution 4.0 International License.
Read Full License

Additional Declarations: Competing interest reported. This study was funded by Google. Y.C., J.P., S.P., R.H., and D.R. are employees of Alphabet and may own stock as part of the standard compensation package. K.V. and A.S. were interns at Google when the study was performed. S.B. has received funding from Google as part of a collaboration agreement unrelated to this paper. The remaining authors declare no competing interests.

Global Geographic, Seasonal, Environmental and Demographic Drivers of Variations in Longitudinal Cardiac Physiology in 5 million Fitbit Users

Katarina Vukosavljević[1,3], Abram Schönfeldt[1,4], Justin Phillips[1], YongSuk Cho[1], Tingting Zhu[3], Shwetak Patel[1,7], Soren Brage[6], Robert Harle[1,5] and Daniel Roggen[1,2]

[1]Google Research, Mountain View, CA, USA, [2]School of Engineering & Informatics, University of Sussex, Falmer, UK, [3]Institute of Biomedical Engineering, University of Oxford, Oxford, UK, [4]Nuffield Department of Population Health, University of Oxford, Oxford, UK, [5]Department of Computer Science and Technology, University of Cambridge, Cambridge, UK, [6]IMS Epidemiology, University of Cambridge, School of Clinical Medicine, Cambridge, UK, [7]Paul G. Allen School of Computer Science and Engineering, University of Washington, Seattle, WA, USA

Resting Heart Rate (RHR) and Heart Rate Variability (HRV) are key biomarkers of cardiovascular health and fitness, but they are typically measured only opportunistically during clinical visits or studies. These sporadic observations make it challenging to identify population-level trends or understand how geographic, environmental and seasonal factors influence cardiac physiology globally. Past research has been limited to small cohorts in selected countries, focusing primarily on RHR while largely overlooking HRV. The widespread adoption of consumer wearables, capable of continuous heart-rate monitoring, makes it possible to finally model and understand these variations on a global scale, but requires a unique access to large volume longitudinal data.

Here, we present the first worldwide models describing the influence of objective, external drivers on cardiac physiology variation, using longitudinal data from 4.9 (RHR) and 2.1 (HRV) million consenting Google Health (Fitbit) users collected across 217 countries globally throughout 2022, representing an unprecedented 60 million person-months dataset. We employ Linear Mixed-Effects models to quantify seasonal (month, day length), geographical (longitude, latitude), and environmental (mean, maximum, and minimum temperature) effects on RHR and HRV while adjusting for demographics (age, sex). We use a novel, automated model search framework across five stages that systematically ablates included drivers, driver encodings, and interaction terms across 20 candidate models per metric. Retaining the best specifications at each stage ensures optimal model parsimony and explanatory power for both RHR and HRV individually.

Our results reveal stable external drivers of RHR variations, and for the first time, of HRV variations as well. For both measures, the optimal model included age, sex, month, longitude, latitude, and minimum and maximum temperature, explaining 5.3% of the population-level variance in RHR and 21.0% in HRV. The magnitude of these fixed effects aligns with previous large-scale physiological studies on sleep, confirming that while these environmental signals are subtle, they represent meaningful and robust population-level drivers. By isolating these drivers, this study provides the first global, monthly-level models for cardiac physiology. Crucially, our modelling framework enables the estimation of physiological variation even in data-sparse regions. Additionally, it provides valuable context for personalised, AI-driven health recommendations in future health assistants, and for normalising disparate national health survey data to a common reference.

1. INTRODUCTION

Resting Heart Rate (RHR) and Heart Rate Variability (HRV) are autonomic biomarkers of cardiovascular health and cardiovascular disease (CVD) [1–7]. Changes in RHR and HRV have both been associated with mortality risk [3, 6, 8] and mental stress [9–13], whilst also functioning as biomarkers of cardiorespiratory fitness [4, 14] driven primarily by shifts in physical activity [15].

Consumer wearable devices enable the continuous measurement of these vital signs across millions of individuals in free-living conditions [16], remotely and non-invasively [17, 18], which ensures continuity in scenarios when in-clinic measurements are restricted, such as during global pandemics

Corresponding author(s): roggen@google.com

[19], or in remote settings lacking traditional medical infrastructure [17, 20]. The accuracy of RHR and HRV wearable sensing also continues to improve as technology advances, and approaches clinical gold standards [17, 21–24]. Continuous wearable sensing underpins recent efforts towards AI-driven, personalised health and fitness insights and automated health assistants [20, 25–30]. However, deploying these tools safely across diverse populations requires establishing rigorous normative baselines, which is currently lacking on a global scale. Traditionally, RHR and HRV have been collected opportunistically during hospital visits or localized clinical studies, which are constrained in time and geography [31]. To build reliable global models, we must characterise normal cardiac fluctuations and untangle their external drivers to distinguish benign environmental adaptations from pathological stress or acute health decline.

Prior smaller-scale studies have established that demographic characteristics influence cardiac physiology. Specifically, women consistently exhibit a higher RHR than men [32–35], and RHR typically follows a non-linear trajectory that increases through middle age, peaking around 45 – 50 years, followed by a gradual decline [32, 33]. The largest scale study to address this question to date ($\sim 92,000$ users), though from one country only (USA), found that these baseline demographic characteristics account for about 6% of population-level variance in RHR [33]. In contrast, while sex-based differences in HRV are prominent in younger cohorts, they become negligible around 45–50 years old and HRV declines significantly with age, reflecting a universal reduction in autonomic flexibility across the lifespan [1, 32, 36, 37].

Beyond demographics, cardiac physiology is driven by additional factors. Individual baseline differences in both RHR and HRV are predominantly influenced by health and behavioural determinants, including BMI [33, 38–40], sleep metrics such as midsleep variability [33, 40, 41], physical activity levels [38, 39, 41], menstrual cycle phase [38], substance use like alcohol and smoking [38, 41], mental health [41], and chronic conditions [38, 41]. These variables, specifically age, sex, BMI, and sleep duration, explain approximately 10% of cardiac variance in RHR [33] (USA; $n = 92,457$), whereas age, sex, BMI, and physical activity account for 19% [38] (location not specified; $n = 28,175$). For HRV, age, sex, BMI, and physical activity explain 15% of population variance [38]. These illustrate the complexity of capturing the dynamics of cardiac variations [42].

Additional external drivers which have been identified include seasonality, although research has historically produced mixed and often conflicting results. On one hand, early controlled studies identified significant winter shifts in cardiac metrics, documenting winter decreases in HRV among specialised cohorts such as adult men [43, 44] and asthmatic children [45], alongside winter elevations in the RHR of smokers [46]. On the other hand, separate investigations reported weak or entirely non-existent seasonal variations in frequency-domain HRV metrics among healthy participants [45, 47], or leaving evidence of consistent RHR fluctuations largely confined to isolated subgroups [46]. This lack of consensus reflects the limitation of prior research, which relied on small, single-country cohorts, across regions such as Israel [44, 46], Russia [43], Japan [45], and Denmark [47].

Beyond seasonal cycles, cardiac measures have been found to be modulated by a wide range of other external drivers. These include pandemic-related lockdown stringency [40], latitude-modulated variations [40, 48], and opposite trajectories between the Northern and Southern hemispheres [40, 48]. Furthermore, environmental factors such as day length, air pollution, altitude [49, 50], ambient temperature [51–54], and solar-geomagnetic activity [55, 56] have also been linked to physiological adaptations. The impact of these environmental factors is often context-dependent. For instance, while ambient temperature exposure is inversely associated with HRV during spring and summer in some cohorts, these findings are not universally supported, with some studies in distinct climates reporting no significant effects [39, 51].

Table 1 summarises studies using wearable or sensor devices that have collected longitudinal

cardiac measures to investigate at least one external driver of cardiac variation (RHR or HRV). Among these, four large-scale wearable studies have analysed temporal patterns in RHR. Two global analyses with Oura ring users revealed seasonal variations [40, 48]. These findings are corroborated by two US studies: Fitbit data captured a statistically significant ~ 2 bpm fluctuation between January and August [33], and SleepImage rings documented a mean heart rate elevation of approximately 2.5 bpm during winter months [57]. Temporal variations were modelled as season [57], month [33, 40], and day (descriptive) [48]. Two studies investigated weather-related factors: ambient temperature in [39, 57], and heat exposure and precipitation in [39]. Finally, two studies looked at geolocation and observed hemispheric differences [40, 48] and latitude differences [40].

While all wearable studies from Table 1 utilise unconstrained, free-living data, their analytical approaches differ. The temporal trajectories were modelled using linear mixed-effects models (LMEs) with user-specific random intercepts in Koch et al. [39] and country-specific random intercepts in Ong et al. [40]. Vazquez et al. [57] tracked baseline changes using ANCOVA and multiple linear regressions, adjusting for age as a continuous covariate. Altini and Plews [38] pooled longitudinal data to fit cross-sectional linear regressions, determining the variance explained by demographics and calculating effect sizes using Cohen's d. Lastly, Koskimäki et al. [48] and Quer et al. [33] did not model the data, instead aggregating user measurements into population-level descriptive statistics and statistical comparisons of means. Relying on raw descriptive data severely limits generalisation, as simple aggregation cannot establish normative baselines in data-sparse regions; conversely, a statistical model resolves this limitation by enabling spatial and temporal interpolation.

Despite the work to date, our understanding of RHR and HRV variations on a global scale is still incomplete. As shown in Table 1, research predominantly focuses on RHR, with only one cross-sectional analysis investigating HRV using a time-domain measure (the root mean square of differences of R-R intervals or rMSSD) [38]. Furthermore, only one study has modelled temporal resolutions finer than quarterly intervals [40], preventing a deeper understanding of how cardiac measures fluctuate throughout the year. Existing literature tends to evaluate environmental drivers in isolation, which fails to reflect the complexity of real-world exposure and hinders any systematic evaluation of their relative contributions. Because these factors are intrinsically linked, independent analysis often yields confounded estimates that larger-scale datasets with broad coverage can help disentangle and clarify. Furthermore, a heavy reliance on cohorts from Western, high-income nations limits the generalisability of findings across diverse global climates and socio-economic contexts [39].

In summary, previous wearable studies, listed in Table 1, have been restricted to investigating simple temporal variations or hemispheric differences, with the largest prior work examining 113,000 Oura ring users across 20 countries to relate RHR to pandemic lockdown stringency [40]. While sleep architecture has been extensively characterised at scale [58–63], a comparable longitudinal analysis of cardiac physiology variation that accounts for diverse external drivers and global-scale geographical representation remains absent. Current isolated approaches fail to capture the complex interplay between demographic, spatial, and environmental drivers, so they leave a critical gap for multiparametric modelling powered by a truly global dataset.

Table 1 | **Summary of related work using longitudinal wearable or sensor data to investigate at least 1 external, objective driver of cardiac variation.**

Author	Method	Target	Location	N	Population	Duration	Model	Drivers Considered	Findings	Cohort
Koch et al. [39]	Withings Pulse HR	Nocturnal HR	Burkina Faso	119 / 46	50.3% male, age: 43 ± 13	2021–22	Linear Mixed-Effects	External (Heat Index, temperature, precipitation)	Decreased sleep duration with increased temperature. Nighttime HR showed no sign. correlation with heat.	General Population
Koskimäki et al. [48]	Oura Ring	RHR	Global	57,278	64% male, age: maj. [30–50]	2016–19	Descriptive	Temporal & Geographic (Macro-seasonality, hemisphere trajectory)	2–3 bpm difference between summer/winter. Trajectories opposite by hemisphere.	General Population
Quer et al. [33]	Fitbit Smart Watches	RHR	USA	92,457	37.4% male, age: 45.8 ± 14.4	2016–18	Statistical comparisons of means	Temporal (Monthly cycles)	RHR varies by age, sex, BMI, and sleep. ~2 bpm difference between July and January.	General Population
Altini and Plews [38]	HRV4Training Mobile app	RHR & HRV	Not specified	28,175	80.0% male, age: 37 ± 12	5 years	Linear Models	Cross-sectional traits (Demographics, BMI, PA)	Sex, PA, age, and BMI explain 19% of variance in RHR and 15% in HRV.	General Population
Vazquez et al. [57]	SleepImage Ring	Mean, min, max HR	USA	2,386	50.9% male, age: 52.4 ± 14.2	2022–25	ANCOVA and Linear Regression	Temporal & Climatic (Seasonal trends, ambient temperature)	2.5 bpm baseline difference between summer/winter. Seasonal variations are stable across multiple years.	Suspected sleep-disordered breathing
Ong et al. [40]	Oura Ring	RHR	Global (20 countries)	~ 113,000	Predominantly male, mean age 35–45y	2019–20	Multilevel Linear Mixed-Effects	Temporal, Lockdown stringency (Monthly trends)	RHR decreased with lockdown severity, driven by sleep variability. Seasonal effects lowered RHR in summer, with hemispheric and latitudinal phase-dependencies.	General Population

Abbreviations: ANCOVA: Analysis of Covariance; BMI: Body Mass Index; bpm: Beats Per Minute; HR: Heart Rate; HRV: Heart Rate Variability; PA: Physical Activity; RHR: Resting Heart Rate; T1D: Type 1 Diabetes.

In this work, we leverage longitudinal physiological data from over five million consenting Google Health (Fitbit) users across the globe collected during 2022 to create a worldwide model characterising the external, objective, globally and continuously measurable drivers on cardiac physiology. Using monthly-level wearable data, we employ a novel, automated model search framework using Linear Mixed-Effects (LME) modelling approach to systematically investigate the effects of age, sex, temperature (average, minimum, and maximum), season (month of the year, day length), and location (longitude and latitude) on the global variations in resting heart rate (RHR) and heart rate variability (HRV) (rMSSD). Our key contributions are as follows:

- **Large-scale Data**: We utilise a massive global dataset of over five million users and more than 60 million user-months spanning 217 countries and territories (as defined by ISO 3166-1). To our knowledge, this represents the largest real-world longitudinal dataset dedicated to monthly-averaged population-scale RHR and HRV tracking analysed to date. Beyond supporting robust modelling, this scale provides valuable insight into the global baseline distributions and real-world characteristics of long-term wearable tracking.
- **Comprehensive Multiparametric Modelling**: We employ LMEs to establish the first global, age- and sex-stratified monthly population-level trends for both RHR and HRV. Notably, this is the first model of temporal variations in HRV.
- **External and Seasonal Effects**: We isolate and quantify the independent and interactive effects of objective, invariant, external drivers and their interplay on cardiac measures, including geolocation (latitude and longitude), ambient temperature (monthly-averaged daily mean, maximum, and minimum), and seasonality (day length, month of the year).
- **Systematic Incremental Validation**: We detail an automated incremental modelling framework consisting of five nested stages, designed to ensure optimal model parsimony and explanatory power. Through systematic ablation testing, we validate the contribution of each driver, progressing from a baseline model comprising only demographic predictors, to more complex models including additionally season, then geolocation, temperature, finally yielding a full model including all five types of predictors.
- **Framework for Global Health Applications**: Our model enables the estimation of normative cardiac trends in data-sparse regions. This is particularly important for future AI-driven health insights and health assistants, such as those developed by large consumer wearable companies which need to be deployable on a global scale, including in regions where historical wearable data is sparse.
- **Country-level Physiological Correlation:** We demonstrate that residual physiological variations align with country-level identifiers. This provides early insights into localised socio-cultural and determinant of health determinants.

2. RESULTS

2.1. Descriptive Statistics

Our analysis is based on a global dataset of consenting users of wearable devices made by Google and Fitbit. We extract and analyse the Resting Heart Rate (RHR) (Table 2) and Heart Rate Variability (HRV) (Table 3) datasets separately. These datasets are obtained after applying minimal data cleaning and data-availability inclusion and exclusion criteria (Section 4).

Across both RHR ($N = 4,833,797$) and HRV ($N = 2,081,733$) datasets, there is a majority of women (67.1% and 66.0%, respectively), with a mean participant age of 45.9 ± 14.8 years for RHR and 44.0 ± 14.1 years for HRV. The substantially smaller size of the HRV dataset is primarily due to more stringent measurement and baseline constraints during sleep (see Section 4.1.1). In total,

participants contributed roughly 40.4 million user-months for RHR and 16.6 million for HRV, with a median of 9 [IQR: 5, 12] monthly records for both metrics.

A stratified breakdown across five latitude bands defined by 30° geographic intervals (Mid South, South Tropics, North Tropics, Mid North, Far North, see Tables 2 and 3) shows that demographic composition remains consistent within each of the bands. As expected, the vast majority of participants are situated in the Northern Hemisphere (specifically the Mid North band, representing 85.4% of RHR and 87.8% of HRV cohorts), reflecting the global population distribution.

Table 2 | **Participant demographics and physiological characteristics across latitude bands during 2022 for the Resting Heart Rate cohort.** Data are presented as mean ± s.d., median [IQR], or counts (n). To adjust for the varying number of months contributed by each participant due to individual device wear patterns and to prevent duplicate counting across geographic regions, each participant is assigned to their single most common latitude band across all user-months. We calculate the individual longitudinal mean for RHR before computing and reporting the population averages.

Sex	Variable	Overall	Mid South (−60 to −30°)	S. Tropics (−30 to 0°)	N. Tropics (0 to 30°)	Mid North (30 to 60°)	Far North (60 to 90°)
Overall							
	n (participants)	4,833,797	152,992	100,945	405,118	4,126,430	48,312
	Age (years)	45.9 ± 14.8	44.5 ± 14.9	44.4 ± 14.7	43.8 ± 14.4	46.2 ± 14.8	45.4 ± 15.5
	User-months, median [IQR]	9 [5, 12]	9 [4, 12]	8 [4, 12]	7 [4, 11]	10 [5, 12]	10 [5, 12]
	User-months, total	40,360,093	1,218,375	772,587	2,969,729	34,993,692	405,710
	RHR (bpm)	67.7 ± 8.1	67.9 ± 8.0	68.6 ± 8.2	70.0 ± 8.5	67.4 ± 8.1	66.2 ± 7.7
Male							
	n (participants)	1,590,911	47,595	33,580	175,572	1,320,899	13,265
	Age (years)	46.8 ± 15.1	46.0 ± 15.3	45.8 ± 15.1	44.3 ± 14.7	47.2 ± 15.0	47.0 ± 15.6
	User-months, median [IQR]	9 [5, 12]	8 [4, 12]	8 [4, 12]	7 [4, 11]	9 [5, 12]	9 [5, 12]
	User-months, total	12,891,550	374,760	255,402	1,261,760	10,890,579	109,049
	RHR (bpm)	65.9 ± 8.4	65.7 ± 8.2	66.5 ± 8.4	69.1 ± 8.9	65.4 ± 8.2	64.2 ± 7.9
Female							
	n (participants)	3,242,886	105,397	67,365	229,546	2,805,531	35,047
	Age (years)	45.4 ± 14.6	43.8 ± 14.6	43.6 ± 14.5	43.3 ± 14.1	45.7 ± 14.6	44.8 ± 15.4
	User-months, median [IQR]	10 [5, 12]	9 [5, 12]	8 [4, 12]	7 [4, 11]	10 [5, 12]	10 [5, 12]
	User-months, total	27,468,543	843,615	517,185	1,707,969	24,103,113	296,661
	RHR (bpm)	68.6 ± 7.8	68.8 ± 7.7	69.6 ± 7.9	70.7 ± 8.1	68.4 ± 7.8	66.9 ± 7.5

2.1.1. Resting Heart Rate

The RHR dataset includes over 4.8 million users globally with a population-wide mean RHR of 67.7 ± 8.1 bpm (Table 2). As illustrated in Figure 1A, RHR exhibits a characteristic non-linear trajectory across the human lifespan: RHR rises gradually throughout young adulthood, peaks in mid-life around age 45 (≈ 68.7 bpm), and subsequently declines in older age. Sex-specific age trajectories (detailed in Supplementary Figure A.1) and Table 2 show that women have a higher RHR than men (≈ 2.2 bpm at age 45). Tropical cohorts exhibit higher baseline RHRs (Figure 1B; 70.0 ± 8.5 bpm in Northern Tropics) compared to polar cohorts (66.2 ± 7.7 bpm in Far North). Demographic composition varies moderately across latitude bands, which can either mitigate or amplify regional cardiovascular baselines if these were evaluated from the raw data directly. For example, the raw tropical RHR is elevated (+2.6 bpm) despite a higher male proportion (43.3% in tropical vs. 32.0% in temperate zones). Because men generally have lower RHRs than women, this demographic mix should theoretically pull the raw tropical average down. Instead, the tropical RHR remains the highest globally, showing that environmental factors can shape physiological patterns even before adjusting for demographics.

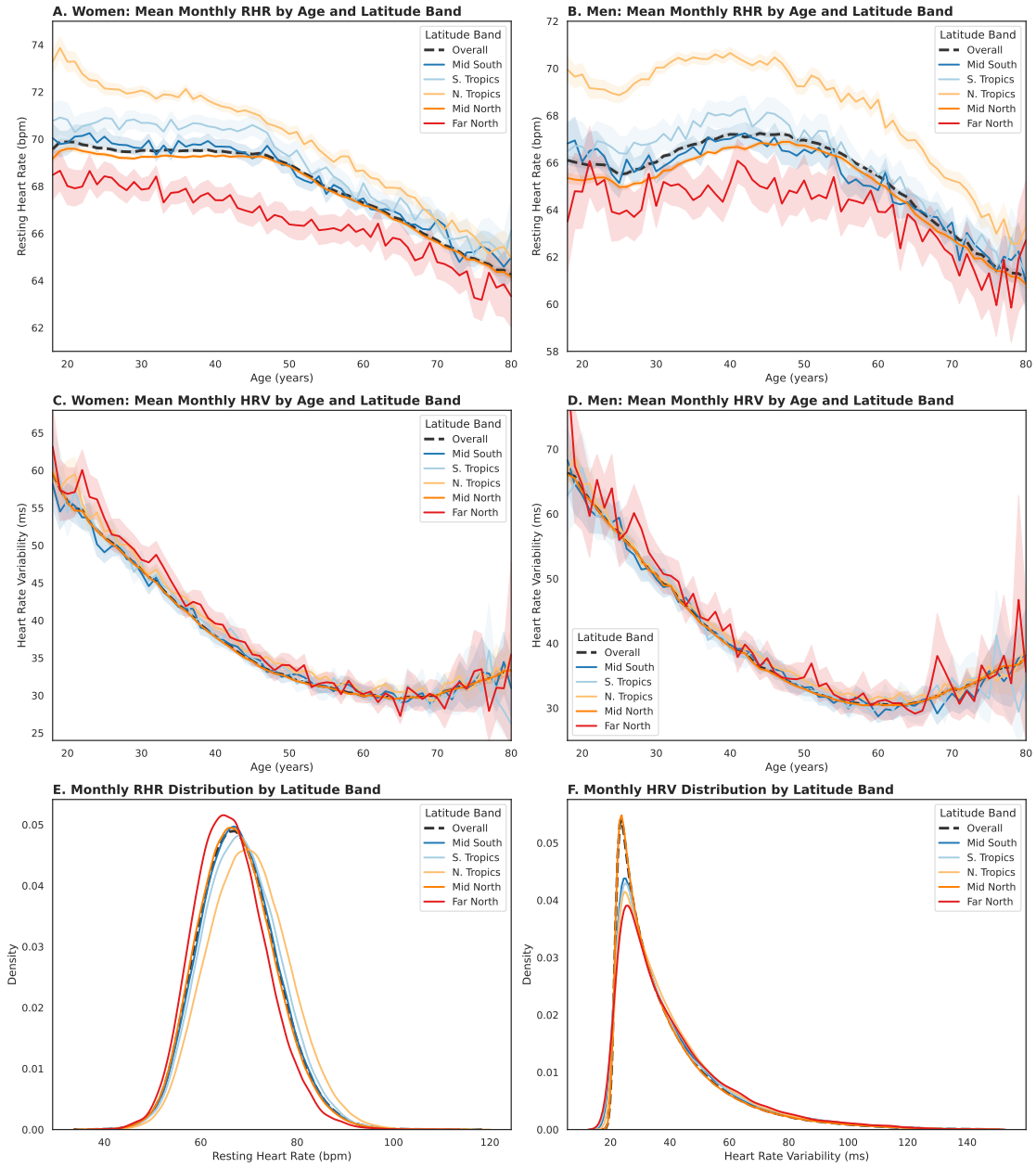

Figure 1 | **Population demographic distributions across latitude bands and overall.** (Row 1) Resting Heart Rate (RHR) cohort. (A) Women and (B) Men: Mean monthly user-averaged RHR vs. age (years), with 95% CI shaded. (Row 2) Heart Rate Variability (HRV) cohort. (C) Women and (D) Men: Mean monthly user-averaged HRV vs. age (years), with 95% CI shaded. (Row 3) Population density distributions. (E) Population density distribution of user-averaged monthly RHR and (F) Population density distribution of user-averaged monthly HRV by latitude band. Overall populations are shown as dashed black lines, while individual latitude bands are shown in colour.

Table 3 | **Participant demographics and physiological characteristics across latitude bands during 2022 for the Heart Rate Variability dataset.** Data are presented as mean ± s.d., median [IQR], or counts (n). To adjust for the varying number of months contributed by each participant due to individual device wear patterns and to prevent duplicate counting across geographic regions, each participant is assigned to their single most common latitude band across all user-months. We calculate the individual longitudinal mean for HRV before computing and reporting the population averages. As HRV (RMSSD) is right-skewed, descriptive summary statistics are reported as median [IQR] across latitude bands.

Sex	Variable	Overall	Mid South (−60 to −30°)	S. Tropics (−30 to 0°)	N. Tropics (0 to 30°)	Mid North (30 to 60°)	Far North (60 to 90°)
Overall							
	n (participants)	2,081,733	61,998	35,192	134,678	1,827,217	22,648
	Age (years)	44.0 ± 14.1	42.4 ± 14.2	42.8 ± 14.2	43.4 ± 14.0	44.1 ± 14.1	43.2 ± 14.5
	User-months, median [IQR]	9 [5, 12]	8 [4, 12]	8 [4, 11]	7 [4, 11]	9 [5, 12]	9 [5, 12]
	User-months, total	16,631,582	480,687	267,746	998,660	14,702,156	182,333
	HRV (ms)	33.1 [26.0, 45.9]	34.0 [26.4, 47.3]	34.0 [26.4, 47.8]	35.1 [27.2, 48.2]	32.9 [25.9, 45.6]	34.9 [26.9, 49.0]
Male							
	n (participants)	706,765	20,703	12,397	61,914	604,988	6,763
	Age (years)	45.3 ± 14.5	44.2 ± 14.7	44.8 ± 14.5	44.0 ± 14.2	45.5 ± 14.5	45.3 ± 14.8
	User-months, median [IQR]	8 [4, 12]	8 [4, 12]	8 [4, 11]	7 [4, 11]	8 [4, 12]	8 [4, 12]
	User-months, total	5,484,201	157,410	93,485	449,420	4,730,381	53,505
	HRV (ms)	33.8 [26.2, 47.2]	34.5 [26.5, 48.4]	34.1 [26.3, 48.4]	35.8 [27.6, 49.2]	33.6 [26.1, 46.9]	35.2 [27.0, 49.8]
Female							
	n (participants)	1,374,968	41,295	22,795	72,764	1,222,229	15,885
	Age (years)	43.3 ± 13.9	41.5 ± 13.8	41.7 ± 13.8	42.8 ± 13.8	43.4 ± 13.9	42.2 ± 14.3
	User-months, median [IQR]	9 [5, 12]	8 [4, 12]	8 [4, 11]	8 [4, 12]	9 [5, 12]	9 [5, 12]
	User-months, total	11,147,381	323,277	174,261	549,240	9,971,775	128,828
	HRV (ms)	32.8 [25.9, 45.2]	33.7 [26.4, 46.8]	34.0 [26.4, 47.5]	34.4 [26.9, 47.2]	32.6 [25.8, 45.0]	34.8 [26.9, 48.7]

2.1.2. Heart Rate Variability

The HRV dataset encompasses over 2.0 million users globally. The monthly rMSSD exhibits a marked right-skew (Figure 1), so its central tendency is characterised by the median and interquartile range (Table 3). Physiological trajectories across age and latitude bands are illustrated in Figure 1. As shown in Figure 1C, HRV exhibits a steep, parabola-like decline across adulthood, dropping rapidly from early young adulthood (≈ 54 ms at age 20) before flattening and rising again in older age (≈ 26 ms at age 65+). Sex-specific trajectories, Figure 1, show that men generally exhibit higher baseline HRV compared to women during young adulthood, with the differences diminishing in older age (see Table 3). Median HRV values remain stable across latitude bands, ranging from 32.9 ms [IQR: 25.9, 45.6] in Mid North to 34.9 ms [IQR: 26.9, 49.0] in Far North (Table 3). As with RHR, the HRV dataset is also majority female (66.0%).

2.2. Linear Mixed-Effects Modelling

RHR and HRV are modelled independently using a Linear Mixed-Effects (LME) framework we develop to perform an automated optimal model search through five incremental stages, explained in detail in Section 4.2. In this work, we investigate and model the effects of the following external objective drivers of variation: 1) geolocation (latitude and longitude), 2) seasonality (month of the year and day length), and 3) environmental temperature (mean, minimum and maximum).

As a summary, in Stage 1, we establish a demographic baseline using age and sex. Stage 2

introduces month of the year and day length to explore the optimal method of modelling temporal seasonality. Stage 3 then incorporates geolocation into the seasonal baseline, whereas Stage 4 expands the seasonal model to include temperature metrics. Finally, Stage 5 integrates all predictors (age, sex, month, latitude, longitude, and residualised temperature) to evaluate the full model. To ensure optimal model structure, we perform systematic ablations within each stage across included drivers, driver encodings, and interactions. In total, we test 20 candidate models for each physiological variable, using the best model from each stage as a basis for the following stage. In this framework, month of the year is modelled as a continuous, circular variable using cosinor fitting to capture seasonal oscillations through both fundamental and second-order harmonic terms.

Given the large dataset size, almost all estimated parameters achieve formal statistical significance ($p < 0.001$). Consequently, we focus our analysis on interpreting physiological effect sizes and relative model parsimony achieved across the stages.

Across both RHR and HRV, the full joint model (Stage 5, Model 5.3, as defined in Section 4.2) has the optimal goodness-of-fit (minimising both AIC and BIC) and achieves the highest marginal R^2 and lowest root mean square error (RMSE). While the inclusion of all three classes of external drivers (temporal seasonality, geolocation, and environmental temperature) is optimal for both RHR and HRV, the underlying physiological mechanisms and optimal model structures differ. Specifically, the RHR model requires a quadratic age interaction with seasonal harmonics and models latitude non-linearly ($\phi + \phi^2$), whereas the HRV model is best represented by a linear age-season interaction and a linear latitude term (ϕ). The realised selection paths and specific variables included at each stage are detailed in Table 8 and Table 9 in the Methodology section.

Our automated model search highlights steady and statistically significant improvements in model performance across stages, as detailed in Table 4 (Section 2.2.1) and Table 5 (Section 2.2.2). Across both RHR and HRV, the unexplained within-person noise (residual SD) is minimised consistently from Stage 1 to Stage 5, confirming that the added fixed effects successfully capture systematic intra-individual variations. Similarly, the stable between-person baseline variation (participant intercept SD) is reduced in the final joint models, while the conditional R^2 remains high, indicating that these individual baselines account for the majority of the variance. Although the absolute increases in marginal R^2 and decreases in RMSE and variance components are small, they are highly statistically significant due to our large dataset size. Crucially, because our automated pipeline selects winning models based on BIC, which penalises complexity, rather than directly optimising for marginal R^2, the consistent maximisation of marginal R^2 along the selected paths serves as independent verification of the framework's validity.

Our incremental staging framework allows us to identify and resolve multicollinearity between seasonal and temperature drivers. Fixed-effect coefficients for demographics and spatial variables remain highly consistent across stages, indicating robust estimation. However, when raw temperatures are introduced in Stage 4, the circannual calendar-month amplitude collapses to near-zero for both RHR and HRV. This indicates that the raw temperature variables absorb the broader seasonal variance due to their strong annual correlation. Stage 5 disentangles this relationship by introducing residualised temperatures (T^{res}), which orthogonalise acute thermal effects from the latitudinal and calendar-month baseline. This re-emerges the independent seasonal rhythm (peaking in January for RHR and July for HRV) alongside the acute effects of local thermal deviations (see Table 4 and Table 5). Without this incremental comparison, the distinct influences of geographic baselines, seasonal trajectories, and local monthly temperature deviations would have remained undetected.

2.2.1. Resting Heart Rate

The optimal model (Stage 5, Model 5.3; Table 4 with the standardised fixed-effect coefficients (Std. β)) includes all five groups of different predictor variables: demographics (age a, quadratic age a^2, sex s, and age-sex interactions), seasonal harmonics (circannual h_1, semi-annual h_2), geolocation (latitude ϕ, latitude squared ϕ^2, longitude harmonics $\lambda_{\sin}, \lambda_{\cos}$), latitudinal seasonal moderation ($\phi \cdot h_1$, $\phi^2 \cdot h_1$), and residualised temperatures ($T^{\text{res}}_{\max}$, $(T^{\text{res}}_{\max})^2$, $T^{\text{res}}_{\min}$, $(T^{\text{res}}_{\min})^2$ and harmonic moderation). The complete unstandardised parameter estimates and raw coefficients of the harmonic drivers across all tested models are listed in Supplementary Table A.3 (unstandardised) and Table A.4 (standardised).

Baseline inter-individual differences accounted for a high proportion of variance, as evidenced by the adjusted Intraclass Correlation Coefficient (adj ICC ≈ 0.914). While the results show that all of our included fixed-effects account for 5.33% of the population-level variations by the marginal R^2, the conditional $R^2 = 91.8\%$ and RMSE = 2.252 bpm indicates that the overall model fits well. This means that the vast majority of RHR variance is driven by stable, person-specific baselines (such as genetics, cardiovascular health, and fitness). The per-person random intercepts account for a baseline variation of 7.81 bpm and residual within-person noise spanning 2.40 bpm.

We found the baseline mean RHR to be 67.63 bpm for the average participant (female baseline: 68.48 bpm, male baseline: 65.91 bpm), fitting the empirical data well, see Table 2. Men exhibit on average a 2.57 bpm lower RHR compared to women (95% CI: $[-2.59, -2.56]$). We find the sex-age interaction to be non-linear in age, with a 2-SD increase in age leading to (Std. $\beta = +6.20$ bpm, 95% CI: $[6.11, 6.29]$) and age squared to (Std. $\beta = -8.74$ bpm, 95% CI: $[-8.83, -8.65]$), both modulated by sex ($a \cdot s = +6.66$ bpm, $a^2 \cdot s = -6.03$ bpm).

The population-level main seasonal effects are best modelled with cosinor fitting on the month of the year rather than day length. We find a circannual wave (h_1) peaking in January (0.20 bpm) and a semi-annual wave (h_2) peaking mid June (0.17 bpm). RHR variation by latitude captures significant curvature ($\phi = 0.09$ bpm, $\phi^2 = -0.57$ bpm) implying a decrease of RHR from the equator towards the poles, which we also observe in the raw data (Table 2). Additional latitudinal effects stem from its interaction with season, with the strongest coming from the fundamental harmonic: $\phi \cdot h_1 = 0.51$ bpm (peak in February) and $\phi^2 \cdot h_1 = 0.38$ bpm (peak in August). For longitude we capture a minor cyclical effect of low amplitude (~ 0.05 bpm at -26.5 °, going through the Americas), suggesting we don't observe a West-East trend. We further observe best model fit with temperature terms including their squares, with a positive effect of residualised maximum temperature ($T^{\text{res}}_{\max} = +0.28$ bpm, 95% CI: $[0.27, 0.29]$) and a stronger negative effect of residualised minimum temperature ($T^{\text{res}}_{\min} = -0.50$ bpm, 95% CI: $[-0.51, -0.49]$). Similarly to latitude, we observe seasonal modulation by both harmonics in both $T^{\text{res}}_{\max}$ and $T^{\text{res}}_{\min}$.

2.2.2. Heart Rate Variability

The optimal model (Stage 5, Model 5.3; Table 5 with the standardised fixed-effect coefficients (Std. β)) includes all five groups of different predictor variables: demographics (age a, quadratic age a^2, sex s, and age-sex interactions), seasonal harmonics (circannual h_1, semi-annual h_2), geolocation (latitude ϕ, longitude harmonics $\lambda_{\sin}, \lambda_{\cos}$), latitudinal seasonal moderation ($\phi \cdot h_1$), and residualised temperatures ($T^{\text{res}}_{\max}$, $(T^{\text{res}}_{\max})^2$, $T^{\text{res}}_{\min}$, $(T^{\text{res}}_{\min})^2$ and harmonic moderation). Due to the log-normality of HRV, the fixed-effects coefficients (Std. β) and variance diagnostics (RMSE, residual noise SD, and participant intercept SD) are expressed as proportional percentage variations ($(e^{\beta} - 1) \times 100\%$ and $(e^{\sigma} - 1) \times 100\%$) to enable physiological interpretability. The complete unstandardised parameter estimates and raw coefficients of the harmonic drivers across all tested models are listed in Supplementary Table A.7 (unstandardised) and Table A.8 (standardised).

Table 4 | **Linear Mixed-Effects Model Estimates for Resting Heart Rate (RHR) across the incremental stages. Values represent standardised fixed-effect parameter estimates (Std. β) in beats per minute ([bpm]) per 2-SD predictor shift alongside their 95% confidence intervals.**

Predictors	Stage 1 (Demo) [bpm]	Stage 2 (Season) [bpm]	Stage 3 (Spatial) [bpm]	Stage 4 (Temperature) [bpm]	Stage 5 (Joint) [bpm]
Fixed Effects: Demographics					
(Intercept)	67.65 [67.64, 67.66]	67.64 [67.64, 67.65]	67.65 [67.65, 67.66]	67.71 [67.70, 67.72]	67.63 [67.63, 67.64]
a (Age)	6.21 [6.12, 6.30]	6.21 [6.12, 6.30]	6.19 [6.10, 6.28]	6.23 [6.14, 6.32]	6.20 [6.11, 6.29]
a^2	-8.73 [-8.82, -8.64]	-8.73 [-8.82, -8.64]	-8.73 [-8.82, -8.64]	-8.77 [-8.86, -8.68]	-8.74 [-8.83, -8.65]
s (Sex)	-2.53 [-2.54, -2.51]	-2.53 [-2.55, -2.52]	-2.57 [-2.59, -2.56]	-2.52 [-2.53, -2.50]	-2.57 [-2.59, -2.56]
$a \cdot s$	6.66 [6.47, 6.85]	6.67 [6.48, 6.86]	6.65 [6.47, 6.84]	6.68 [6.49, 6.87]	6.66 [6.48, 6.85]
$a^2 \cdot s$	-6.06 [-6.25, -5.87]	-6.06 [-6.25, -5.87]	-6.02 [-6.21, -5.83]	-6.07 [-6.26, -5.88]	-6.03 [-6.22, -5.85]
Fixed Effects: Seasonality					
Annual Rhythm (h_1)	–	0.28 [Jan]	0.28 [Jan]	0.04 [Feb]	0.20 [Jan]
Semi-annual Rhythm (h_2)	–	0.16 [5.5m]	0.16 [5.5m]	0.17 [5.9m]	0.17 [5.5m]
Fixed Effects: Spatial Geography					
ϕ (Latitude)	–	–	0.12 [0.11, 0.13]	–	0.09 [0.08, 0.10]
ϕ^2	–	–	-0.46 [-0.47, -0.46]	–	-0.57 [-0.58, -0.56]
$\lambda_{\sin}$ (Longitude)	–	–	-0.03 [-0.04, -0.03]	–	0.04 [0.03, 0.05]
$\lambda_{\cos}$	–	–	-0.12 [-0.12, -0.11]	–	-0.02 [-0.03, -0.01]
$\phi \cdot h_1$	–	–	0.49 [Feb]	–	0.51 [Feb]
$\phi \cdot h_2$	–	–	0.06 [3.7m]	–	0.13 [4.8m]
$\phi^2 \cdot h_1$	–	–	0.35 [Aug]	–	0.38 [Aug]
$\phi^2 \cdot h_2$	–	–	0.14 [5.8m]	–	0.04 [0.9m]
Fixed Effects: Temperature					
$T_{\max}/T_{\max}^{\text{res}}$	–	–	–	0.26 [0.23, 0.28]	0.28 [0.27, 0.29]
$T_{\max}^2/(T_{\max}^{\text{res}})^2$	–	–	–	-0.08 [-0.10, -0.06]	-0.09 [-0.11, -0.08]
$T_{\min}/T_{\min}^{\text{res}}$	–	–	–	-0.78 [-0.80, -0.76]	-0.50 [-0.51, -0.49]
$T_{\min}^2/(T_{\min}^{\text{res}})^2$	–	–	–	0.16 [0.15, 0.17]	-0.06 [-0.07, -0.05]
$T_{\max} \cdot h_1/T_{\max}^{\text{res}} \cdot h_1$	–	–	–	0.70 [Jan]	0.45 [Jul]
$T_{\max} \cdot h_2/T_{\max}^{\text{res}} \cdot h_2$	–	–	–	1.17 [2.7m]	0.39 [2.6m]
$T_{\min} \cdot h_1/T_{\min}^{\text{res}} \cdot h_1$	–	–	–	0.34 [Jan]	0.24 [Jan]
$T_{\min} \cdot h_2/T_{\min}^{\text{res}} \cdot h_2$	–	–	–	0.55 [5.6m]	0.20 [5.9m]
Variance Components					
Residual SD [bpm]	2.414	2.403	2.400	2.400	2.398
Intercept SD [bpm]	7.839	7.839	7.809	7.840	7.808
Adjusted ICC	0.913	0.914	0.914	0.914	0.914
Model Fit Diagnostics					
RMSE [bpm]	2.267	2.257	2.254	2.254	2.252
BIC (ML)	207602873	207258823	207128522	207179659	207094560
AIC (ML)	207602749	207258637	207128149	207179162	207093878
Log-Likelihood (ML)	-103801367	-103629307	-103564051	-103589549	-103546895
Marginal R^2 / Conditional R^2 [%]	5.100 / 91.777	5.178 / 91.857	5.312 / 91.831	5.208 / 91.878	5.327 / 91.838

Notes: Values represent standardised fixed-effect parameter trajectories (Std. β) and their 95% confidence intervals. Estimates are presented in beats per minute [bpm] and represent absolute changes, including the Intercept which represents the baseline mean in bpm. Seasonal harmonic pairs ($\cos, \sin$) are combined into Circannual/Semi-annual Amplitudes with peak calendar months (Phase) indicated in brackets [Month]. *Italic values indicate coefficients that are NOT statistically significant ($p \geq 0.05$, 95% CI includes zero)*. Unstandardised estimates (Est.) and complete parameter grids across all models are provided in Supplementary Materials.

Similarly to RHR, the baseline inter-individual differences of HRV accounted for a high proportion of variance (adj ICC ≈ 0.891). The demographics and external drivers capture 21.03% (marginal R^2) of the population-level variance, and the conditional R^2 = 91.4% and RMSE = 11.73% indicates that the overall model fits well. This means that the overall variance is driven by both by demographics and external effects, as well as by stable, person-specific baselines. The per-person random intercepts account for a baseline variation of 40.165% and residual within-person noise spanning 12.567%.

The intercept shows the baseline geometric mean HRV to be 35.30 ms for the average participant (female baseline: 34.72 ms, male baseline: 36.46 ms), fitting the empirical data well (Table 3). We again find the sex-age relationship to be non-linear, with a 2-SD increase in age leading to a linear decline (Std. β = −68.26%, 95% CI: [−68.45%, −68.08%]) and a quadratic rebound (Std. β = +125.83%, 95% CI: [124.51%, 127.15%]), both modulated by sex ($a \cdot s$ = −29.92%, $a^2 \cdot s$ = +36.19%).

Seasonal effects are best modelled with cosinor fitting on the month of the year rather than day length, See Supplementary Table A.6. The population average shows a circannual wave (h_1) peaking in July with an amplitude of 1.79% (≈ 0.63 ms at baseline) and a semi-annual wave (h_2) peaking in mid-March with an amplitude of 0.94% (≈ 0.33 ms at baseline). Interestingly, we find that HRV is very weakly modulated linearly by latitude, and the relationship is statistically non-significant (ϕ = −0.04%, 95% CI: [−0.10%, 0.01%]), as observed in the raw demographics (Table 3). Instead, the latitudinal variation is expressed through its seasonal interaction, with a strong circannual latitudinal moderation peaking in August ($\phi \cdot h_1$ = 2.60%, ≈ 0.92 ms at baseline). For longitude, we capture a minor cyclical effect of low amplitude (∼ 1.02%, ≈ 0.36 ms at baseline, phase: 19.5°, going through Europe and Africa), suggesting there is no meaningful West-East trend. Temperature effects are best modelled using residualised temperatures and their quadratic terms. The dominant thermal drivers are the linear effect of residualised maximum temperature ($T_{\max}^{\text{res}}$ = +2.02%, 95% CI: [1.93%, 2.11%]; ≈ 0.71 ms at baseline) and the quadratic effect of residualised minimum temperature ($(T_{\min}^{\text{res}})^2$ = +2.10%, 95% CI: [2.01%, 2.19%]; ≈ 0.74 ms at baseline), indicating a pronounced U-shaped sensitivity to minimum residualised temperature. The main linear effect of residualised minimum temperature is statistically non-significant ($T_{\min}^{\text{res}}$ = −0.08%, 95% CI: [−0.16%, 0.00%]). Both temperature metrics show significant seasonal moderation by both annual and semi-annual harmonics.

Table 5 | **Linear Mixed-Effects Model Estimates for Heart Rate Variability (HRV) across the incremental stages. Values represent standardised fixed-effect parameter estimates (Std. β) evaluated in log-transformed space ($\ln$ HRV) and transformed to percentage changes ([%], $(e^{\beta}-1)\times 100$) per 2-SD predictor shift alongside their 95% confidence intervals.**

Predictors	Stage 1 (Demo) [%]	Stage 2 (Season) [%]	Stage 3 (Spatial) [%]	Stage 4 (Temperature) [%]	Stage 5 (Joint) [%]
Fixed Effects: Demographics					
(Intercept)	35.44 [35.43, 35.46]	35.45 [35.44, 35.47]	35.57 [35.55, 35.59]	35.40 [35.39, 35.42]	35.30 [35.28, 35.32]
a (Age)	-68.11% [-68.29%, -67.92%]	-68.14% [-68.33%, -67.96%]	-68.22% [-68.40%, -68.03%]	-68.18% [-68.37%, -68.00%]	-68.26% [-68.45%, -68.08%]
a^2	124.71% [123.40%, 126.03%]	124.80% [123.49%, 126.12%]	125.60% [124.29%, 126.92%]	125.08% [123.77%, 126.40%]	125.83% [124.51%, 127.15%]
s (Sex)	5.15% [5.05%, 5.25%]	5.22% [5.12%, 5.33%]	5.10% [5.00%, 5.20%]	4.96% [4.86%, 5.07%]	5.02% [4.92%, 5.12%]
$a \cdot s$	-29.71% [-30.55%, -28.85%]	-29.76% [-30.60%, -28.90%]	-29.90% [-30.75%, -29.05%]	-29.86% [-30.71%, -29.00%]	-29.92% [-30.77%, -29.06%]
$a^2 \cdot s$	35.87% [34.23%, 37.52%]	35.87% [34.23%, 37.52%]	36.11% [34.48%, 37.77%]	36.14% [34.50%, 37.80%]	36.19% [34.55%, 37.85%]
Fixed Effects: Seasonality					
Annual Rhythm (h_1)	–	2.84 [Jul]	2.83 [Jul]	0.45 [Aug]	1.79 [Jul]
Semi-annual Rhythm (h_2)	–	1.31 [2.2m]	1.31 [2.2m]	0.93 [2.5m]	0.94 [2.5m]
Fixed Effects: Spatial Geography					
ϕ (Latitude)	–	–	-0.36% [-0.41%, -0.31%]	–	*-0.04% [-0.10%, 0.01%]*
$\lambda_{\sin}$ (Longitude)	–	–	1.16% [1.11%, 1.20%]	–	0.96% [0.91%, 1.00%]
$\lambda_{\cos}$	–	–	0.43% [0.39%, 0.48%]	–	0.34% [0.29%, 0.39%]
$\phi \cdot h_1$	–	–	2.75 [Aug]	–	2.60 [Aug]
$\phi \cdot h_2$	–	–	0.70 [1.8m]	–	0.42 [2.1m]
Fixed Effects: Temperature					
$T_{\max}/T^{\text{res}}_{\max}$	–	–	–	4.81% [4.59%, 5.04%]	2.02% [1.93%, 2.11%]
$T^2_{\max}/(T^{\text{res}}_{\max})^2$	–	–	–	-0.42% [-0.59%, -0.25%]	0.18% [0.09%, 0.28%]
$T_{\min}/T^{\text{res}}_{\min}$	–	–	–	-0.84% [-0.96%, -0.72%]	*-0.08% [-0.16%, 0.00%]*
$T^2_{\min}/(T^{\text{res}}_{\min})^2$	–	–	–	1.63% [1.55%, 1.71%]	2.10% [2.01%, 2.19%]
$T_{\max} \cdot h_1/T^{\text{res}}_{\max} \cdot h_1$	–	–	–	4.76 [Jul]	2.13 [Aug]
$T_{\max} \cdot h_2/T^{\text{res}}_{\max} \cdot h_2$	–	–	–	6.42 [5.7m]	2.58 [5.3m]
$T_{\min} \cdot h_1/T^{\text{res}}_{\min} \cdot h_1$	–	–	–	1.92 [Aug]	0.62 [Jan]
$T_{\min} \cdot h_2/T^{\text{res}}_{\min} \cdot h_2$	–	–	–	4.05 [2.4m]	1.52 [2.5m]
Variance Components					
Residual SD (proportional) [%]	12.884%	12.639%	12.591%	12.587%	12.567%
Intercept SD (proportional) [%]	40.133%	40.175%	40.142%	40.204%	40.165%
Adjusted ICC	0.886	0.890	0.890	0.890	0.891
Model Fit Diagnostics					
RMSE [%]	12.022%	11.794%	11.749%	11.746%	11.727%
BIC (ML)	14670789	15194418	15302380	15304927	15353515
AIC (ML)	14670906	15194593	15302658	15305395	15354085
Log-Likelihood (ML)	-7335461	-7597309	-7651348	-7652730	-7677082
Marginal R^2 / Conditional R^2 [%]	20.595 / 90.927	20.911 / 91.263	21.017 / 91.319	21.002 / 91.342	21.032 / 91.356

Notes: Values represent standardised fixed-effect parameter trajectories (Std. β) and their 95% confidence intervals. Estimates are presented in percentage changes ([%], $(e^{\beta}-1)\times 100$), except for the Intercept which represents the baseline mean in ms. Seasonal harmonic pairs (cos, sin) are combined into Circannual/Semi-annual Amplitudes with peak calendar months (Phase) indicated in brackets [Month]. *Italic values indicate coefficients that are NOT statistically significant ($p \geq 0.05$, 95% CI includes zero).* Unstandardised estimates (Est.) and complete parameter grids across all models are provided in Supplementary Materials.

3. DISCUSSION

Our findings confirm well-established demographic variations in resting cardiac physiology while characterising their non-linear trajectories across the adult lifespan (Figure 1). Consistent with prior clinical and wearable studies [32–35, 38], women in our Fitbit cohort exhibit a higher RHR than men across all age groups. The previously largest wearable study by Quer et al. ($n = 92,457$; US) observes this sex-based RHR difference to be ~ 3.3 bpm. For our US cohort, we similarly observe a 3.2 bpm difference between men and women, though the LME model isolates a sex difference of 2.57 bpm worldwide, which may suggest that uncontrolled confounding factors, such as age and our external drivers, can bias demographic estimates. Furthermore, in Quer's analysis, RHR initially rises across early adulthood before declining for both sexes. While we observe the same trend for men in our cohort, we find that the mean RHR for US women remains stable or gradually decreases before it experiences a more pronounced decline. This relationship is captured by the age-by-sex quadratic interaction terms in our model (Supplementary Tables A.2 and A.6) and accounts for 5.1% of RHR population-level variation (close to the 6% reported by Quer et al. [33]). Lastly, while Altini and Plews [38] reported no direct linear relationship between RHR and age overall, our findings provide further evidence that age and sex should be modelled together through a quadratic age by sex interaction, as we find that age does meaningfully moderate RHR. Including the nonlinear interaction increases the explained variance from 4.3% to 5.1%, Table 4 and Supplementary Table A.2.

For HRV, we find sex-based differences that are prominent in younger cohorts but become negligible around 45–50 years old as HRV declines significantly across the lifespan, Figure 1, a trend that our model identifies and quantifies as explained in Section 2.2.2. This reflects a universal reduction in autonomic flexibility with age and aligns with previous work [1, 32, 36, 37, 64]. However, we find that age and sex alone explain 20.6% of population-level variance (Supplementary Table A.6), whereas prior work by Altini and Plews [38] reported that baseline characteristics (age, sex, BMI, and physical activity) account for only 15% of HRV variance. This discrepancy stems partly from methodological differences. Specifically, the previous study modelled age and sex linearly and independently, whereas our results demonstrate that incorporating quadratic age-by-sex interactions increases the explained HRV variance from 18.3% to 20.6% (Supplementary Table A.6). Furthermore, although they noted no direct association between HRV and sex, our global data confirms clear sex-based differences in younger adult cohorts. Despite this, prior studies provide evidence that our findings still fit within theoretical bounds as they have found that 31 – 64 % of population-level variance in HRV in middle-aged men is driven by genetics [65, 66] alone. Across both metrics, we find that age is a strong driver of variation in HRV but less so for RHR, agreeing with [32, 38].

Model predictions by age group and sex (Figure 2) across both RHR and HRV show that the models fit the data well across all subgroups. However, we note two fitting peculiarities around the start and end of the year. In January, the model underestimates the mean RHR for all apart from the youngest cohort (18–29) and slightly overestimates the HRV for women in January apart from the oldest cohort (68–78). In December, across both sexes and under 48 years old, the model underestimates the mean HRV. Both observations are possibly explained by holiday-related behavioural changes, such as altered sleep patterns, increased alcohol consumption, and physical activity changes surrounding the festive season, as was previously suggested in [33, 38, 48].

In order to evaluate how well environmental and demographic trends generalise globally, we visualised model projections against empirical observations. We confirm that the models tracks these monthly trajectories with high fidelity across diverse countries and both hemispheres (Figures 3 and 4) and successfully captures opposing trajectories by hemisphere (Figure 4). In agreement with prior wearable and clinical cohorts, we also observe a clear circannual rhythm characterised by winter elevations in RHR and concurrent decreases in HRV, with the inverse pattern in summer. Specifically,

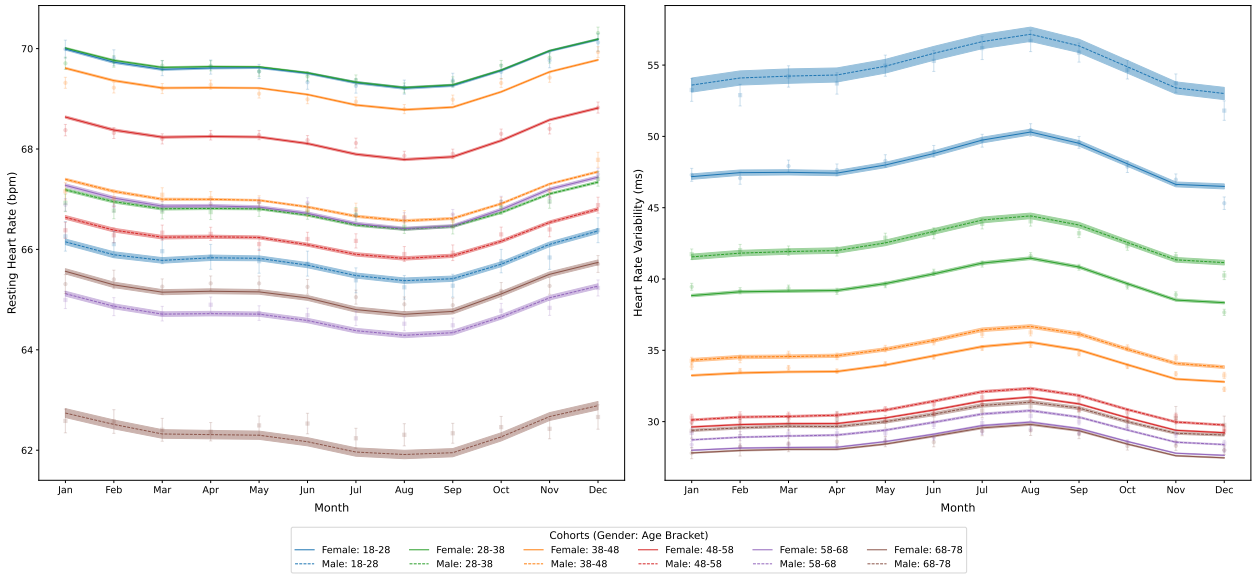

Figure 2 | **Model Fit against Empirical Observations across Demographics.** The plots show the winning models prediction (curves with 95% confidence bands) overlaid on observed monthly means (points with 95% confidence intervals) across age-sex groups for RHR (Left) and HRV (RHR), showing that the LMEs successfully track non-linear trajectories across the cohorts. Observations represent raw trends, and the model predictions include random effects.

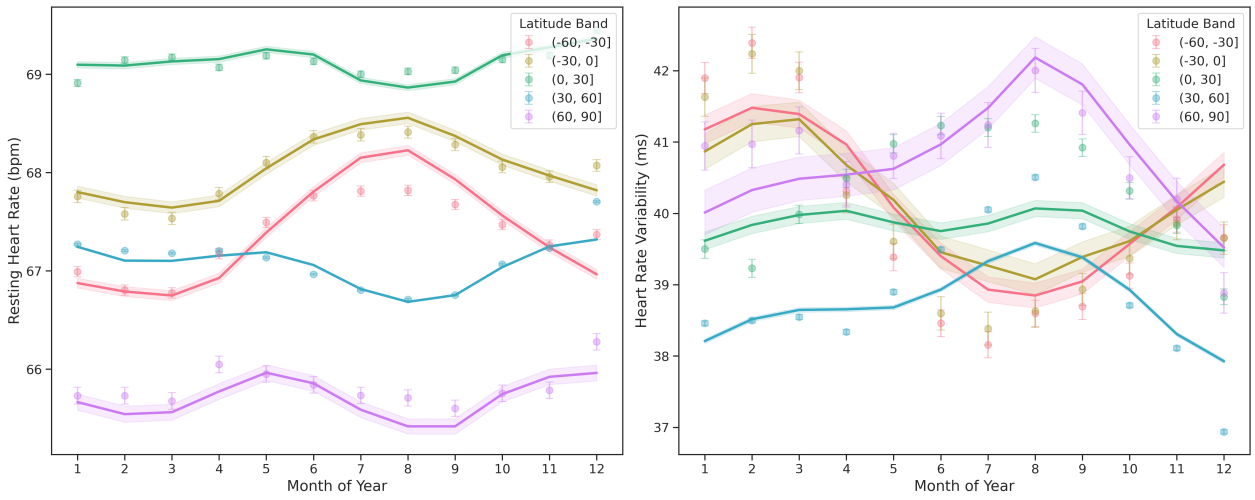

Figure 3 | **Model Fit against Empirical Observations across Latitude Bands.** The plots show the winning model predictions (curves with 95% confidence bands) overlaid on observed monthly means (points with 95% confidence intervals) across latitudinal bands for RHR (Left) and HRV (Right). Observations represent raw trends, and the model predictions include random effects.

RHR peaks during the Northern winter (January) in the US and Japan, peaks during the Southern winter (July–August) in Australia, and remains nearly flat in countries closer to the equator like India (observed difference: 0.21 bpm). Looking deeper into the individual country plots, our US cohort shows an observed winter–summer difference of 0.61 bpm, while Japan and Australia exhibit observed amplitudes of 0.95 bpm and 0.97 bpm, respectively (Figure 4), aligning with latitude-dependent seasonality observations [40].

In contrast to previous large-scale studies that estimated RHR seasonal amplitudes of approximately 1.0 to 1.5 bpm, such as Quer et al. [33] ($\sim$ 1.5 bpm in a US Fitbit cohort) and Koskimäki et al. [48] ($\sim$ 1.0 bpm in Oura ring users across the globe), our global analysis reveals a more muted RHR seasonal amplitude. We observe a summer–winter difference of approximately 0.74 bpm in the Southern Hemisphere and 0.55 bpm in the Northern Hemisphere. While Vazquez et al. [57] reported a higher 2.5 bpm summer–winter difference, this was in a US clinical population with suspected sleep-disordered breathing, which likely inflated the amplitude compared to the general population. Furthermore, the Northern Hemisphere exhibits a slightly greater average difference than the Southern Hemisphere, likely due to a broader latitudinal distribution extending to high latitudes, whereas Southern Hemisphere users only extend to $-60°$. A more detailed country-by-country comparison of observed mean-centred data against Ong et al. [40] is provided in the Supplementary Materials B.4. This comparison reveals a baseline offset between our Fitbit cohort and their Oura cohort, which we primarily attribute to differences in cohort composition: our participants are predominantly female and older (mean age of 45.9 globally), whereas theirs are predominantly male and younger (aged 35 to 45). Despite these distinct demographic profiles and separate device ecosystems, the difference in observed mean-centred data is less than 0.5 bpm in countries with robust sample sizes ($> 5,000$ users). This close alignment across entirely different user populations provides credence that these common findings reflect consistent, universal population-level physiological phenomena, and are not artifacts of specific devices or a heavily biased user base. Beyond data noise, any residual discrepancies are likely driven by month-to-month fluctuations in cohort composition, which is a factor our models account for.

Our findings for HRV show a universal winter-related decline across both hemispheres, with HRV peaking in summer (Figures 4 and 5). This is consistent with Kristal-Boneh et al. [44], who reported a 3.1 ms winter reduction despite measuring mean rMSSD over a 24-hour period rather than our nighttime metric. In our cohort, we observe a winter HRV decrease of 1.21 ms in the US (predicted: 1.63 ms). This winter decline is also documented by Belisheva et al. [43] during the polar night in adolescents residing beyond the Arctic Circle. Lastly, Figure 3 shows that we do not observe latitude-modulated seasonal peaks in HRV, which is confirmed by our model results (Section 2.2.2).

To complement these localised country fits, we also visualised the observed global seasonal differences across the globe (Figure 5). These maps show the observed mean RHR and HRV during each of the four seasons, revealing both seasonal changes for each country, and clear latitude modulation independent of season. For HRV, spatial variations are clear. For instance, in the Americas, countries near the equator maintain a consistently higher mean HRV (indicated by red) than those at higher northern and southern latitudes (blue). For RHR, the maps capture broader hemispheric phase reversals and seasonal differences. These shifts are shown by cyclical colour transitions between light blue and light orange in countries like Australia and Canada. When Canada appears light blue, Australia is light orange, and vice versa, directly showing opposing seasonal dynamics across the northern and southern hemispheres.

A key strength of our modelling is characterising how different cohorts and climates react to residualised temperature (T^{res}) throughout the year, Tables 4 and 5. Residualisation isolates temperature fluctuations from the temperature which would be expected if given solely the latitude and

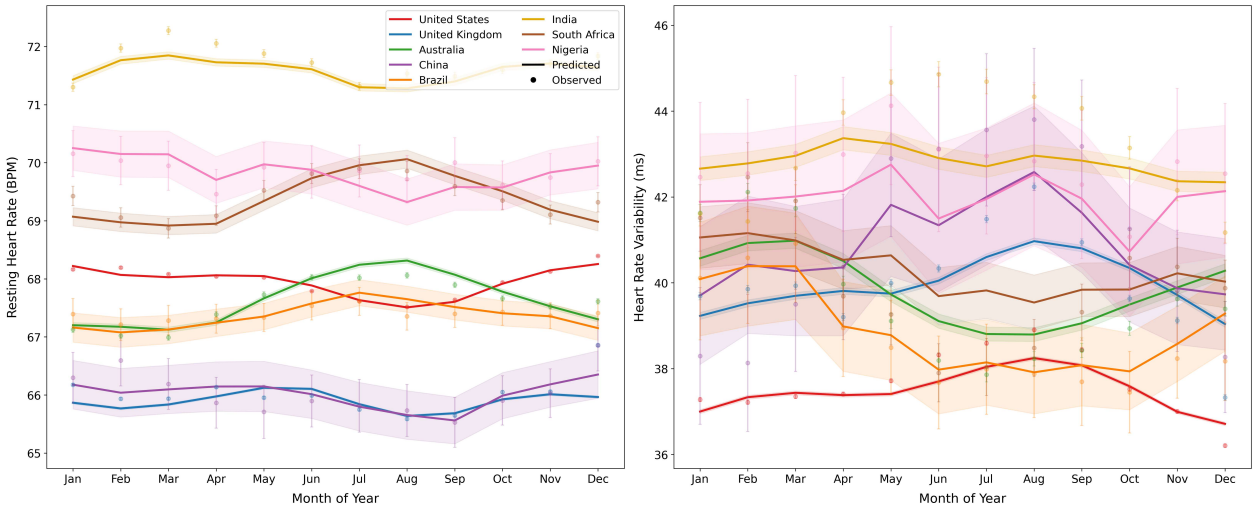

Figure 4 | **Model Fit against Empirical Observations across Selected Countries.** The figure shows observed monthly averages (points with 95% confidence intervals) and model predictions (curves with 95% confidence bands) across eight representative countries (United States, United Kingdom, Australia, China, Brazil, India, South Africa, and Nigeria) for RHR (left) and HRV (right). The trajectories highlight opposing hemispheric phases in temperate regions (e.g., the United States and Australia) (both RHR and HRV), and muted seasonality in tropical and equatorial zones (India, Nigeria) (RHR only). Overall, we observe good tracking across all countries, with the exception of India HRV during the summer, where our model underpredicts, which likely points to other unobserved environmental drivers such as air pollution [67].

month of the year, see Section 4.1.5. By analysing these variations in response to these temperature deviations, we can determine how cardiac regulation adapts to thermal stress, and how this sensitivity is modulated by age.

As illustrated in Figure 6, the within-subject RHR and HRV responses to residualised temperature are highly pronounced in younger cohorts, and decrease in older cohorts. This blunted response, visible as a flatter sensitivity curve in both cardiac metrics during cold conditions, indicates a reduced autonomic reserve to cope with acute environmental stressors in older adults [51].

We find that incorporating both minimum and maximum temperatures explains the model better than using the daily average. Furthermore, temperature affects both metrics and drives U-shaped responses, which we modelled by adding quadratic temperature terms, Table 4 and Table 5. Unlike a study in Burkina Faso [39], our global parametrisation demonstrates that minimum residualised temperature does drive this U-shaped response in RHR. This response may be explained by thermoregulatory cardiac demand and increased physiological stress [51]. This aligns with recent free-living data derived from commercial wearables, which confirms that nocturnal heat exposure induces a shift towards sympathetic dominance, directly elevating heart rate and depressing HRV [54].

To dive deeper into the regional outliers, we analysed the average model residuals globally binned by latitude and longitude grid cells (Figure 7). For both RHR and HRV, the residuals are uniformly distributed across all continents and latitudinal bands. The absence of persistent regional clustering or directional drift confirms that the population-level coefficients represent consistent global trends rather than geographic overfitting or structural model flaws. Nonetheless, examining specific regional outliers where local predictions deviate allows us to identify potential unmeasured confounding factors.

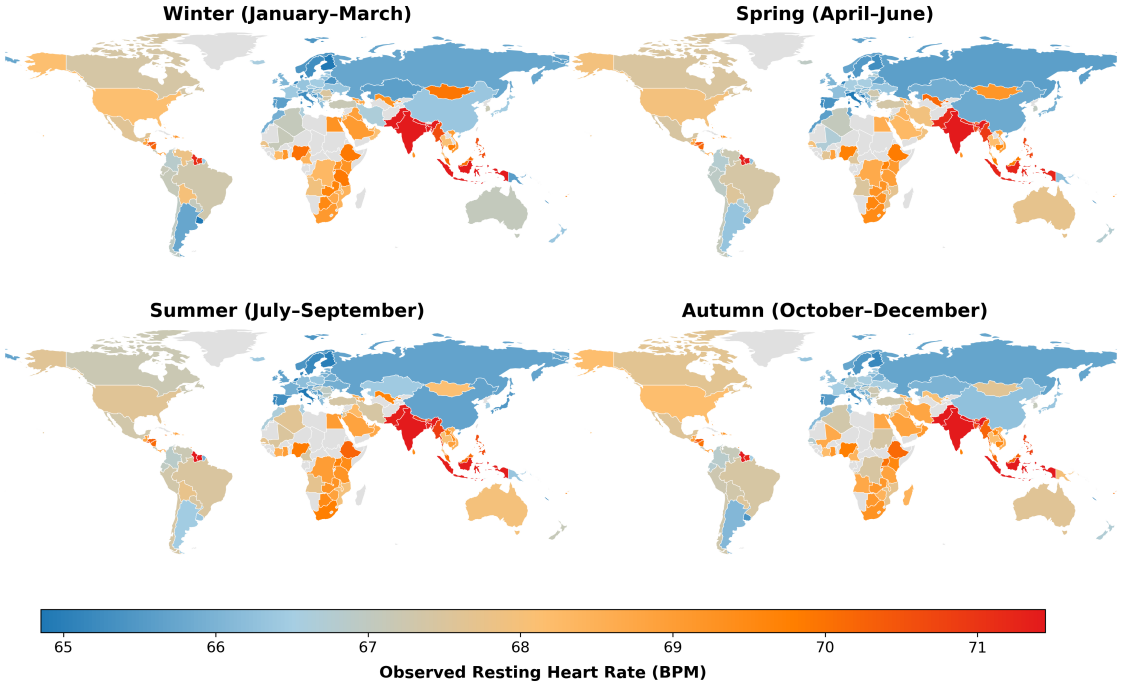

(a) Resting Heart Rate (RHR) Seasonal Variations

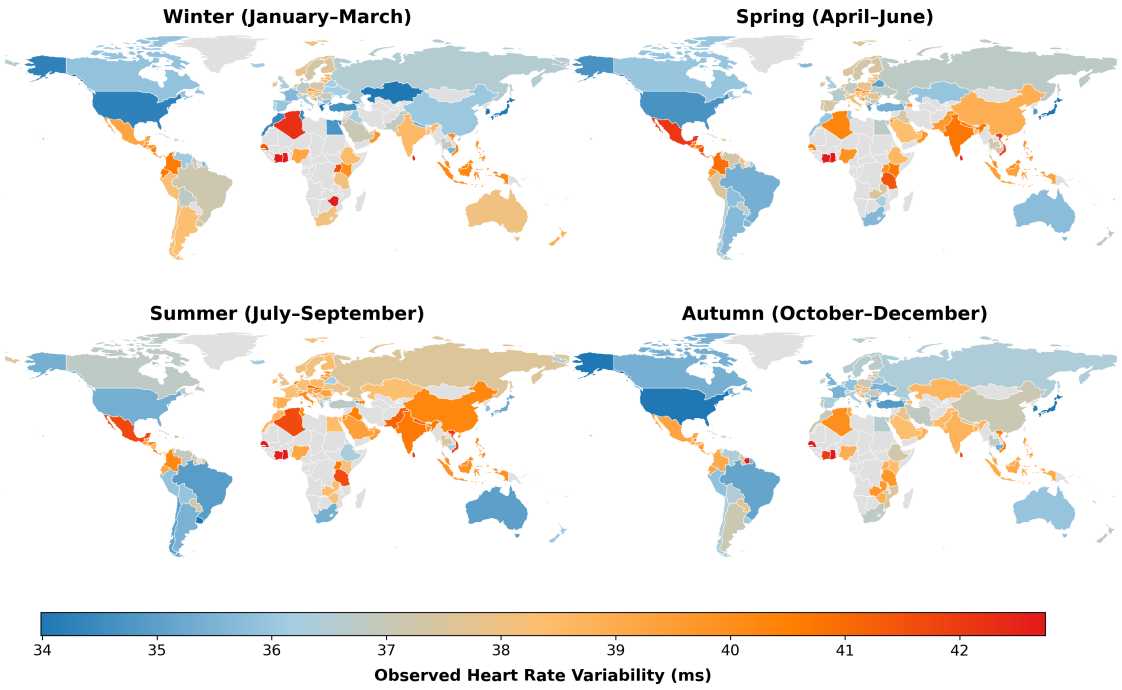

(b) Heart Rate Variability (HRV) Seasonal Variations

Figure 5 | **Global Observed Seasonal Variations across Four Seasons.** The maps show the observed dataset average (a) RHR (bpm) and (b) HRV (ms) during Winter (January – March), Spring (April – June), Summer (July – September), and Autumn (October – December) across countries with ≥ 100 active users. Countries with insufficient data are displayed in grey. The spatial distributions highlight clear latitude-modulated trends, such as elevated HRV near the equator (warmer colours) that decreases progressively at higher latitudes (colder colours), and the opposite for RHR. We also observe elevated RHR and lower HRV in regions with high air pollution [67] and obesity rates [68], like Southern Asia, the US, South America, and Central and South Africa.

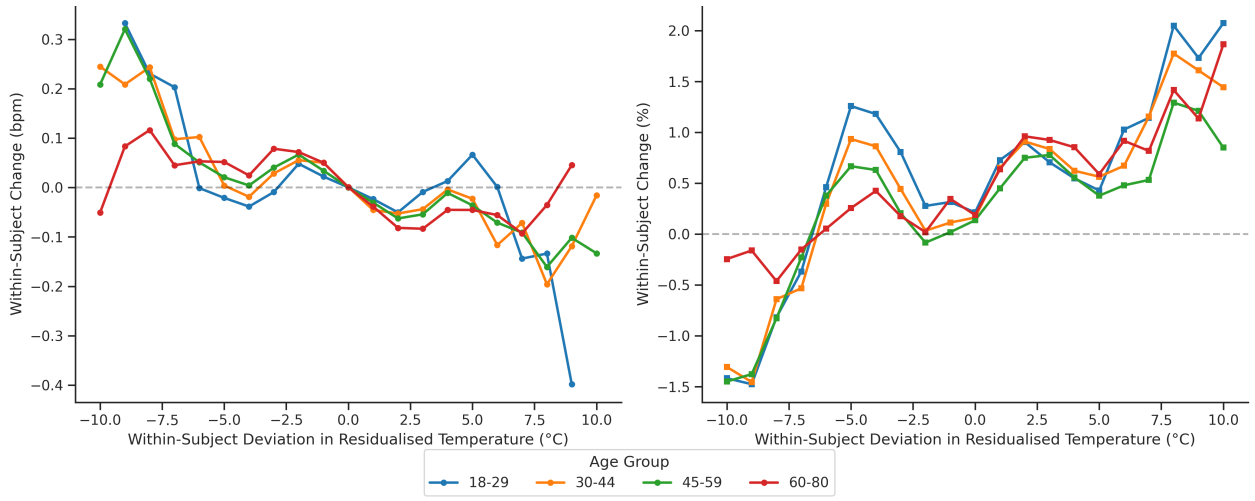

Figure 6 | **Within-Subject Cardiac Sensitivity to Residualised Temperature.** The plots show the within-subject change in (a) resting heart rate (RHR, in bpm) and (b) heart rate variability (HRV, in %) in response to individual-level residualised temperature deviations (deviations from local climatological baselines), stratified by age groups. Younger cohorts exhibit steeper curves (greater autonomic reactivity), whereas the oldest cohort (60–80 years, red) shows a blunted response to residualised temperature, indicating a reduced autonomic reserve.

We observe that the model underestimates population-level RHR in South and South-East Asia, specifically in India, Pakistan, Bangladesh, and Indonesia. We speculate this may be due to increased levels of air pollution, as prior literature shows that both RHR and HRV are acutely sensitive to elevated air pollution [51, 53, 69], which presents severe cardiovascular and public health risks in these regions [67]. Conversely, we observe that the model tends to overestimate RHR in countries such as the United States, Egypt, Saudi Arabia, South Africa, Chile, and Brazil. These nations also exhibit some of the highest global obesity levels [68]. Because obesity causes chronic metabolic strain that heavily impacts cardiovascular health, further work should include and explore BMI as an additional population-level driver. Meanwhile, regions like Europe are consistently underestimated by the global model, which may reflect a baseline counterbalance driven by the lower regional obesity rates and reduced air pollution exposure [67, 68]. We observe similar systemic trends for HRV.

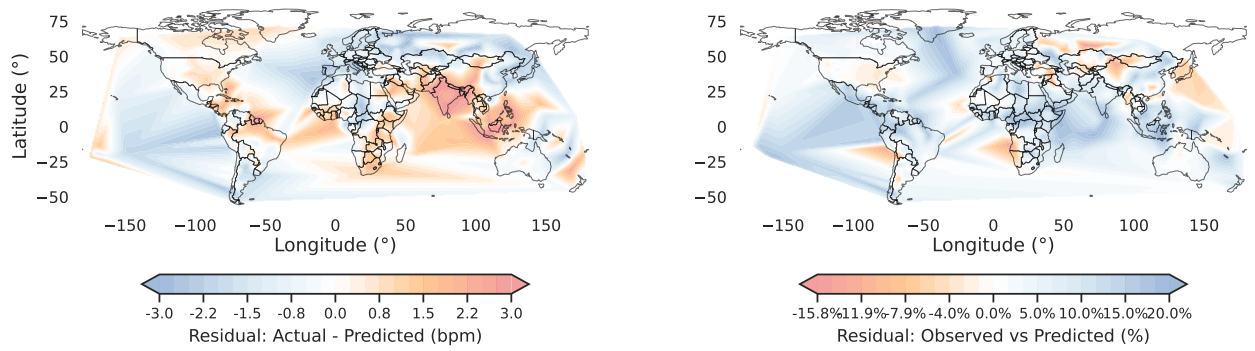

Figure 7 | **Global Distribution of Model Residuals.** The contour plots illustrate the average model residuals (observed minus predicted) binned by latitude and longitude grid cells for RHR (left, in bpm) and HRV (right, in ms). The uniform distribution near zero across the geographic grid demonstrates that the joint models generalise consistently across different regions. We find the global residuals correlate with global obesity [68] and air pollution [67] rates.

Our work has a number of limitations. The participants' demographics (age and sex) are self-reported when they first enrol in the Fitbit ecosystem. We observed suspected instances of reporting errors, specifically the over-representation of birth year 2000. We developed a methodology to address and validate this, which we document in the Supplementary Materials Section A. With this correction applied, the resulting demographics matches what the researchers at Google could corroborate from other data sources, such as internal sales statistics, on an aggregate level.

Similar to some other large-scale wearable datasets, our cohort exhibits a skew toward women [33, 70], younger demographics [71, 72], and Mid-Northern latitude bands [33, 48, 57]. Moreover, we acknowledge potential selection and attrition biases: wearable users often display higher health consciousness than the general population [73], and because our participants explicitly opted in to share their data for research purposes, this engagement may further reflect underlying health-seeking behaviours. Similarly, extended compliance, as shown by our users contributing a median of nine months of data, may also introduce related biases. To mitigate selection bias as much as possible, we purposefully used lenient inclusion criteria (requiring only four data points per month and a minimum participation of two months, see Section 4) and incorporated age-by-sex interaction terms across all models. Although adoption within under-represented low-income regions may skew toward higher-income individuals, these findings would still remain highly relevant for early-adopters of new health AI applications which may share a similar skew, where our results provide useful regional context. Ultimately, as the largest-scale dataset of its kind to date, our cohort encompasses a wide and diverse global user base.

Our study is subject to certain technical and unmeasured constraints. The dataset encompasses a variety of Fitbit and Google device types, ranging from simpler, lower-cost trackers to high-end smartwatches, also reflecting hardware evolution and optical sensing improvements over time [74]. While participant-level random intercepts primarily account for individual baseline differences, they also help accommodate this device-specific variance. Additionally, each participant's location is defined monthly based on where they spend the most time, which may mask transient effects like frequent travel or jetlag. However, we expect these transient effects, alongside our coarse geolocation resolution, to be filtered out as noise given the scale of our datasets.

It is important to note that our primary objective was to determine the impact of external environmental factors on cardiac physiology and establish robust population-level trends. To achieve this, we purposefully restricted our predictors to objective external drivers that are globally and universally accessible, leveraging the available consumer dataset as rigorously and completely as possible using well-validated and widely used sensoring technologies. Like almost all consumer wearable manufacturers at the time, Fitbit did not capture clinical data in 2022, so there was no mechanism to systematically collect medical histories or medication logs. While modern wearables contain multiple sensors, we excluded those that do not currently provide reliable data for population-scale modelling. For instance, although some devices feature an electrodermal activity (EDA) sensor or a photodetector (used for screen brightness) that could theoretically estimate sweat or ambient light exposure, the signal quality from these components remains inconsistent in free-living conditions. Similarly, we used ambient temperature data from local weather stations rather than the devices' internal temperature sensors, which are highly susceptible to noise from body heat and clothing. Consequently, unmeasured clinical confounders, such as underlying cardiovascular disease or medication use, alongside unmeasured environmental factors like air pollution, indoor climate control, or artificial lighting, may contribute to residual regional and individual variation. Similarly, while we do not isolate weekday versus weekend effects or account for transient events like Daylight Saving Time, public holidays, or religious observances, we anticipate these factors are sufficiently mitigated by our study's large scale and monthly resolution. Nonetheless, we encourage future work to explore these dynamics with finer temporal granularity.

Furthermore, our models exclude body mass index (BMI) due to limited data availability (6.5% of the HRV cohort and 7.8% of the RHR cohort) and the risk of introducing selection bias, as self-reporting this metric may strongly correlate with health consciousness. Similarly, we do not incorporate race or socioeconomic indicators (such as income, education, or healthcare access) because as Fitbit does not collect this data. While BMI can further explain population-level variance in cardiovascular metrics [33, 38] and socioeconomic factors may further correlate with it [68], its relationship with health is complex and varies substantially across cultural contexts, suggesting it may better be analysed at a localised, country-specific level to provide accurate regional nuance.

Many individual-level drivers, such as granular behavioural patterns and clinical health status, remain challenging to obtain across consumer ecosystems without dedicated clinical integration and the privacy challenges associated with it and potential reluctance of participants of sharing such information. Nonetheless, as multi-sensor consumer AI health assistants evolve, our methodology serves as a blueprint for future scaling. Building on this foundation, future work could examine how the effects of external factors (month, temperature, and geolocation) vary within specific clinical cohorts, such as patients with cardiovascular disease [45, 46], and investigate whether these nocturnal patterns extend to other physiological states, even those not yet reliably measured by current wearable technologies, that are globally and longitudinally monitored by the WHO (STEPS protocol), for example daytime seated rest or the systolic blood pressure [75]. Research could also incorporate additional external factors, such as local air quality indices [69] or ambient noise [76, 77], to refine the explanatory power of these physiological models in regions where these factors present population-health risks like Pakistan, India, China, or DR Congo [67]. Furthermore, longitudinal analyses should extend across multiple years to evaluate how environmental drivers evolve alongside gradual climatic shifts, while finer temporal granularity could help explore transient factors like holiday schedules [33, 38, 48]. Finally, our framework offers a mechanism for standardising health metrics collected globally to a common reference. Because international studies are often conducted at disparate times and locations, model coefficients can be used to project and harmonise physiological baselines, providing a robust tool to validate data from regions with limited longitudinal coverage against broader global estimates.

Finally, future studies should explore intra-individual sensitivity or resilience to these drivers. While the present study focused on established population-level trends rather than individual-level variation, subsequent research could specifically target these differences to identify which sub-populations are most responsive to environmental change. This includes examining the physiological impact of acute stressors, such as trans-meridian and cross-climate travel, where the abrupt nature of the environmental shift provides a unique opportunity to quantify individual autonomic adaptation.

In conclusion, we present the first global models characterising the demographic and environmental drivers of longitudinal cardiac physiology. Utilising the largest dataset of its kind to date, spanning over five million Fitbit users across 217 countries, we systematically quantified how age, sex, season, geolocation, and temperature shape population-level trends in resting heart rate (RHR) and heart rate variability (HRV). To ensure robust findings, we developed a systematic framework for building the optimal LME model alongside a density-based method to correct for false demographic reporting.

We find that demographics and external drivers account for 5.3% and 21.0% of the population-level variance in RHR and HRV, respectively. These figures quantify the impact of these drivers for the first time and establish a foundational baseline for global cardiac variation. Overall, age and sex trends in our Fitbit cohort closely align with prior work for both metrics. However, accurate analysis requires accounting for the nonlinear, quadratic effect of age and its interaction with sex, and failing to control for these confounding factors significantly biases demographic estimates. The combination of this large-scale dataset and detailed modelling enabled us to capture nuances across the lifespan that

previous models have missed, such as identifying clear sex-based differences in HRV within younger cohorts. Through our incremental approach, we demonstrate that environmental drivers require similarly complex modelling. We find that seasonal variations are better explained using cosinor fitting on the month of the year and geolocation (latitude and longitude), rather than day length. Furthermore, temperature effects must be examined within a latitudinal context using residualised and quadratic terms to accurately capture their physiological impact; specifically, this approach revealed U-shaped responses to both minimum and maximum temperatures across both metrics, with minimum temperatures exerting a stronger effect. Omitting latitude causes raw temperature metrics to absorb spatial variances, leading to uncontrolled confounding that obscures true environmental effects. Notably, while adjusting for geolocation is essential to prevent this confounding, we find that latitude itself has no significant direct effect on HRV, whereas it remains a significant driver for RHR.

Crucially, this work establishes the first global model for HRV, filling a major gap in a field historically focused on RHR. By isolating these population-level baselines, we identify specific new hypotheses for future research, such as investigating whether local factors like obesity and air pollution explain regional deviations from global predictions. Finally, our framework provides a robust mechanism to estimate baselines in data-sparse regions, normalise data reporting to harmonise cross-national studies, and refine future AI-driven health assistants by supplying essential regional context.

4. METHODOLOGY

4.1. Dataset Description & Extraction

For this analysis, we curated a large-scale, global longitudinal dataset of wearable device data (Fitbit trackers and Google smartwatches) and weather data spanning the full 2022 calendar year. We have chosen 2022 as the observation year to allow for a direct comparison to previous work [41, 57, 63] and also because this is the first year in which pandemic-related restrictions were largely phased out. We could not use a more recent year than 2022 due to technical limitations resulting from changes in data storage infrastructure following the Google acquisition of Fitbit. To investigate the relationship between weather and physiological measures, we combined the wearable data (Section 4.1.1) of each participant with the nearest public source of weather data (Section 4.1.2).

Ethics approval for the use of the real-world dataset from Fitbit/Google was granted by the Western Institutional Review Board-Copernicus Group IRB, which classified the research as exempt under 45 CFR 46.104(d)(4).

4.1.1. Wearable Data

All users of Fitbit trackers or Google Pixel Watches are asked whether they consent to their data being used for research purposes when they set up their devices for the first time. The study population consists of those users who provided informed consent for their de-identified data to be used for such purposes, and who met specific inclusion and exclusion criteria. We included all wearable devices by Fitbit and Google equipped with a heart rate sensor to ensure our analysis relied exclusively on objective physiological measures rather than self-reported data.

The wearable dataset consists of the following variables: participant's demographics (age and sex), coarse location on a monthly basis, and daily resting heart rate (RHR) and daily heart rate variability (HRV) measured during the night. As Google researchers, we accessed this data through a Google-internal API, but there exists a public counterpart (Section 4.1.3) providing the same information to external researchers.

Demographics are derived from the self-reported birth year and sex. The cohort is restricted to only female and male users, consistent with the binary sex classifications natively recorded by the Fitbit platform. Age is calculated as the difference between the birth year and the 2022 observation year, strictly excluding individuals under 18 years old to adhere to legal age of consent requirements while retaining users between 18 and 80 years old to ensure a sufficiently sized cohort for robust statistical analysis. Users missing demographic information are excluded from the analysis (2.10% of users).

To preserve user privacy and prevent re-identification, the Fitbit/Google infrastructure handling the data consented for research stores only coarse location data in the form of ISO 3166-2 country and region codes. This corresponds to high-level administrative units e.g., U.S. states or U.K. constituent counties, with the countries illustrated in Figure 8. The location is inferred at the time the user opens the Fitbit application, primarily from the user's IP address. As an additional privacy safeguard, this information is then recorded in a monthly manner as the location where the participant was the most frequently located that month. When curating the data, we assumed that the user remained in this location for the duration of the month. In instances where the location is missing, the corresponding user-month was excluded from the analysis (13.87% of user-month records). The extracted monthly location is subsequently mapped to its centroid's longitude and latitude. The participant geolocation has variable spatial resolution, as the size of the administrative units used in ISO 3166-2 differs across countries. For each user-month, we then also computed the monthly average day length (photoperiod)

using their associated geographic coordinates and the `PyEphem` library [78].

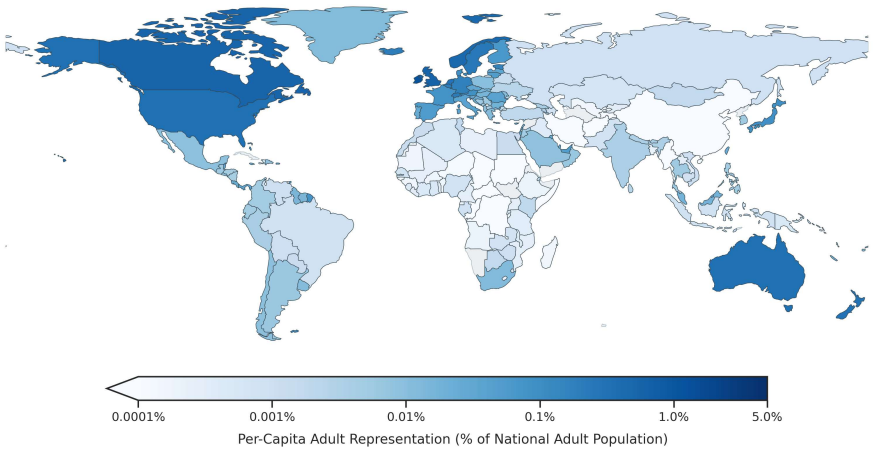

Figure 8 | **Global distribution of the HRV cohort relative to national adult populations.** The plot displays the per capita representation of cohort users for each country (displayed as ISO 3166-2 country codes), calculated as the total number of users divided by the country's adult population. Baseline adult demographic estimates were sourced from the United Nations Population Division [79].

Resting Heart Rate (RHR) and Heart Rate Variability (HRV) are derived from photoplethysmography (PPG) signals processed via proprietary algorithms and are provided as daily estimates. RHR is estimated by taking the lower 10th percentile of the heart rate in periods of no motion, which occur predominantly during the night. If measurements are available only during daytime, a personalised adaptive scaling factor is used to map the RHR to the equivalent which would have been measured if a nighttime measure would have been available. Similarly, HRV is captured during nighttime inactivity and is calculated as the 95th percentile of the root mean square of differences of R-R intervals (rMSSD) across 5-minute epochs, when the R-R interval can be estimated with high confidence from the PPG signal. This ensures that the measured HRV values are captured during deep sleep, and as such represent the user's chronic state, not acute stress. Both internal and external studies have been carried out to validate the obtained Fitbit cardiac measurements [22–24, 80].

This difference in measurement mechanisms and algorithmic constraints explains why the final HRV cohort has less than half the size of the RHR cohort. While RHR can be estimated from daytime rest periods using adaptive scaling, HRV is strictly estimated only during nighttime sleep. Furthermore, the HRV estimation pipeline requires the device to be worn for at least three consecutive nights to establish a personal baseline, and each night's calculation requires a minimum of three hours of continuous trackable sleep with high-confidence PPG signals. Consequently, users who do not wear their trackers to bed regularly, or who have shorter sleep durations, generate daily RHR estimates but fail to produce valid HRV data, thereby reducing the number of users meeting the longitudinal inclusion criteria. To ensure data quality for this analysis, we exclude outliers by capping daily measurements of RHR to 20 to 200 bpm, and HRV to 20 to 200 ms.

For each user, their daily physiological measures are aggregated into monthly averages. To preserve the representative nature of our global cohort and minimise selection bias, we did not impose a minimum daily wear-time requirement nor employed imputation strategies to make up for missing data. However, we exclude user-months with fewer than four valid daily measurements within that month, approximating a minimum of one data point per week. This inclusive threshold was chosen because the large scale of the dataset ensures statistical robustness, whereas more stringent

requirements might inadvertently favour a subset of high-adherence users and thereby introduce bias. The inclusion thresholds we used are in a similar range as previous work [33, 38]. While this threshold does not strictly balance day-of-week representation for lower-adherence users, cohort adherence is generally high, with participants providing an average of 20.3 ± 8.9 days of measurements per month, ensuring day-of-week sampling variation averages out across the population. Finally, to accommodate the Linear Mixed-Effects (LME) modelling approach described in Section 4.2, users were required to have records for at least two months (not necessarily consecutive) to allow for the estimation of within-subject variance.

Finally, like all large-scale wearable datasets, ours is susceptible to noise arising from incorrect demographic self-reporting. To explicitly address this challenge, we introduce a density-based filtering approach. We describe this procedure in the Supplementary Materials Section A and suggest it as a strategy for targeting false reporting in future large-scale digital health studies. We summarise our cohort inclusion and exclusion criteria in Table 6.

Table 6 | Summary of cohort inclusion and exclusion criteria.

Inclusion Criteria	
Consent	Provided consent for the use of de-identified data for research purposes.
Age	Between 18 and 80 years old during 2022.
Sex	Female or Male.
Device type	Any Fitbit tracker or Google Pixel Watch with an active heart rate sensor.
Monthly adherence	At least 4 valid daily measurements of RHR or HRV in a given month.
Longitudinal span	At least two distinct months (not necessarily consecutive) in 2022.
Exclusion Criteria	
Incomplete demographics	Users missing demographic information (birth year or sex).
Missing spatial data	User-months lacking location or weather data.
Physiological outliers	Daily readings falling outside valid physiological limits (RHR < 20 or > 200 bpm; HRV < 20 or > 200 ms).
False reporting	Density-based thinning (Supplementary Materials Section A).

4.1.2. Weather data

Local temperature was sourced from repositories of historical meteorological records including the National Oceanic and Atmospheric Administration (NOAA) (specifically Global Summary of the Day (GSOD) [81], Integrated Surface Database (ISD) [82], Automated Surface Observing Systems (ASOS) [83], Global Historical Climatology Network Daily (GHCN-D) datasets [84]), the United States Climate Reference Network (USCRN) [85], and the United States Environmental Protection Agency (USEPA) [86]. This provides global weather coverage for the year 2022, comprising hourly measurements from 51,148 weather stations across 235 world countries and territories (standardised via ISO 3166-1 alpha-2 codes). Station-level daily temperatures were first aggregated spatially by calculating the daily mean, maximum and minimum for each geographic entity. These daily spatial averages were then aggregated temporally resulting in the the average monthly mean, maximum, and minimum temperatures. These values were subsequently mapped to each user-month record based on the month and the user location, using the geographically closest available weather data. In the rare instances where temperature data were missing for a specific region-month combination, those user-months were omitted from the analysis, excluding 0.02% of the records.

Variable	Scope	Element name
age	profile	user : age
sex	profile	user : gender
location	profile	user : city, user : country
RHR	activity	summary : restingHeartRate
HRV	heartrate	hrv : value : deepRmssd

Table 7 | List of measures accessible from the public Fitbit API corresponding to the variables extracted using the Google-internal API. For the full list of available metrics, please refer to the available documentation [87].

4.1.3. Data Access

The Fitbit data used to curate the dataset for this analysis is also available to other researchers via a public web API [87] in the same or similar form. The differences in the data primarily arise from the additional privacy protections applied to the internal API. For instance, while the public API may provide city-level locations and full birth dates, our internal dataset is limited to ISO 3166-2 regional codes and birth years. Furthermore, the internal dataset records a user's most frequent monthly location, whereas the public API is limited to a single user-set location. Physiological variables are available in the same format across both APIs, and we provide equivalent or proxy variables available through the public API in Table 7.

4.1.4. Curated wearable/weather dataset

The previously described processing steps produce two curated longitudinal datasets, one for RHR and one for HRV. Both datasets consist of monthly observations for the 2022 calendar year and are defined as follows:

$$\mathcal{D} = \{\mathbf{x}_{ij} \mid i = 1, \ldots, N; j = 1, \ldots, 12\}$$

where N is the number of users, $\mathbf{x}_{ij}$ is the monthly observation for user i in month j, represented by the feature vector:

$$\mathbf{x}_{ij} = [y_{ij}, a_i, s_i, m_{ij}, \phi_{ij}, \lambda_{ij}, d_{ij}, T_{ij}, T_{max,ij}, T_{min,ij}]$$

where y is the monthly average physiological measure, a and s are the user's age and sex, $m \in \{1, \ldots, 12\}$ is the observation month (1 = January), $\phi \in [-90, 90]^\circ$ and $\lambda \in [-180, 180]^\circ$ are the latitude and longitude corresponding to the user's monthly location, $d \in [0, 24]$ is the monthly average day length in hours for the associated coordinates, and T, T_{min} and T_{max} are the monthly averages of the daily mean, maximum, and minimum temperatures in degrees Celsius ($^\circ C$), respectively.

4.1.5. Variable Encoding

We standardise all continuous, non-cyclical predictors (specifically: age, temperature, day length, and latitude[1]) by mean-centring and scaling by two standard deviations to ensure model convergence and facilitate direct comparison with the binary predictor (sex) [88]. To handle the periodicity of longitude λ, initially in decimal degrees, we convert it to radians and map to Cartesian components:

$$\lambda_{\sin} = \sin(\lambda \cdot \pi/180), \quad \lambda_{\cos} = \cos(\lambda \cdot \pi/180)$$

[1]Latitude is modelled as a non-cyclical predictor as it is naturally bounded by Earth's poles.

Lastly, to account for the circular nature of the month of the year, we employ techniques from cosinor analysis [89]. Unlike previous work that treats time of the year as a categorical variable limited to seasons [59, 63, 90], we utilise cosinor fitting to model the month of the year as a continuous, circular variable. We represent the month through Cartesian components and we incorporate both fundamental (annual) and second-order (semi-annual) harmonics to capture more complex seasonal patterns, such as bimodal distributions, without implying four distinct annual peaks.

$$m_{\sin_1} = \sin(2\pi m/12), \quad m_{\cos_1} = \cos(2\pi m/12)$$

$$m_{\sin_2} = \sin(2\pi m/6), \quad m_{\cos_2} = \cos(2\pi m/6)$$

When interpreting the fixed effects post-estimation, these Cartesian seasonal components can be back-transformed to derive the amplitude A and phase θ of the seasonal peaks, such as when reporting results in Section 2. The transformation is performed for each harmonic k (where $k = 1$ denotes the fundamental and $k = 2$ the second-order harmonic) as follows:

$$A_k = \sqrt{\beta_{\cos,k}^2 + \beta_{\sin,k}^2}, \; \theta_k = \operatorname{atan2}(\beta_{\sin,k}, \beta_{\cos,k})$$

where $\beta_{\cos,k}$ and $\beta_{\sin,k}$ are the corresponding unstandardised fixed-effect coefficients. These transformations ensure that all predictors are properly scaled and orthogonalised before being incorporated into the fixed-effects component of our linear mixed-effects models.

Thermal Residualisation. We residualise the temperatures to address collinearity with latitude (ϕ)[2] in models incorporating both drivers. For each standardised temperature metric ($T_{c,ij}$, representing mean, maximum, or minimum monthly temperature for user i in month j), we fit a baseline Ordinary Least Squares (OLS) regression incorporating both latitudinal and seasonal components:

$$T_{c,ij} = \alpha_0 + \alpha_1 \phi_{abs,c,i} + \alpha_2 \phi_{c,i} + \sum_{k=1}^{2} \left[\alpha_{3,k} m_{\sin_k} + \alpha_{4,k} m_{\cos_k}\right] + \sum_{k=1}^{2} \left[\alpha_{5,k} m_{\sin_k} \phi_{c,i} + \alpha_{6,k} m_{\cos_k} \phi_{c,i}\right] + T_{ij}^{\text{res}} \quad (1)$$

where $\phi_{c,i}$ represents the standardised signed latitude for user i, $\phi_{abs,c,i}$ is the standardised absolute latitude (modelling the climatological temperature drop away from the equator), $m_{\sin_k}$ and $m_{\cos_k}$ are the harmonic components for order $k \in \{1, 2\}$, and $j \in \{1, \ldots, 12\}$ is the calendar month. The interaction between the annual and semi-annual month harmonics and signed latitude ($\phi_{c,i}$) models the seasonal temperature cycle, capturing the opposite phase of seasons between the Northern and Southern Hemispheres. The resulting residuals (T_{ij}^{res}), representing local thermal deviations from the temperatures expected given the latitudinal gradient and month of the year, were then used in the subsequent Stage 5 (Full) models where both drivers are jointly included as independent variables.

This approach serves a dual statistical and physiological purpose. Statistically, including both raw temperature alongside latitude as independent variables produces severe variance inflation ($GVIF^{1/(2\cdot df)} > 2$), rendering linear mixed-effects parameter estimation numerically unstable. Additionally, introducing interaction terms (e.g., $\phi \cdot T$) further exacerbates design matrix collinearity.

Physiologically, latitude (ϕ) acts as a stable proxy for long-term climatic acclimatisation and photoperiod regimes to which our cohort may have adapted, whereas T^{res} cleanly isolates acute thermal deviations (e.g., unexpected heatwaves or unseasonal cold snaps) relative to local baseline.

[2]Global temperatures naturally decrease from the equator toward the poles, and this spatial correlation can lead to unstable coefficient estimates, inflated standard errors, and model convergence issues.

Finally, the total unresidualised environmental signal is evaluated in full during Stage 4 (Temperature stage), where latitude is absent, and Stage 5 is specifically designed to test whether acute weather deviations (T^{res}) drive physiological seasonality over and above stable geographic baselines.

4.2. Linear Mixed-Effects (LME) Models

We use LMEs to model each physiological variable (RHR, HRV) according to demographic (a, s), external drivers $(\phi, \lambda, d, T_m, T_{max}, T_{min})$, and month of the year (m). We include a random intercept per user, similarly to previous work [39, 59, 90]. Omitting subscripts i, j without loss of generality, the general model with a random intercept is defined as:

$$y = \mathbf{X}\boldsymbol{\beta} + Zu + \epsilon \tag{2}$$

where the fixed effects $\mathbf{X}\boldsymbol{\beta}$ represent the population-level average effects of the design matrix $\mathbf{X} \in \mathbb{R}^{M \times p}$ (where M is the total number of observations across the dataset and p is the number of fixed effects), which includes the transformed predictors and their relevant interaction terms across the repeated observations. The random effect $Zu \in \mathbb{R}^M$ is included as a random intercept for each user $u \sim N(0, \sigma_u^2 I)$ to account for repeated observations clustered within individuals as well as for subject-level heterogeneity, such as baseline differences in health or physical activity levels. Here, $\boldsymbol{\beta} \in \mathbb{R}^p$ is the vector of fixed-effects coefficients we wish to learn, and $Z \in \mathbb{R}$ is the random-effects design matrix linking the random intercept to observations. The residual error $\epsilon \sim N(0, \sigma_\epsilon^2 I)$ represents variations not captured by the mixed-effects as well as the residual noise. Finally, $y \in \mathbb{R}^M$ is the physiological variable (RHR or HRV). Modelling was performed using mean monthly RHR, but for HRV we used the the natural logarithm of the monthly mean (ln HRV) in order to accommodate the highly skewed natural distribution of HRV, which can be seen in Figure 1. As a result, coefficients for the ln(HRV) models represent proportional changes in the original HRV scale, in comparison to the RHR models, where the coefficients reflect absolute 1-unit increases.

4.3. Automated Modelling Framework

We develop a novel, automated model search framework using incremental modelling (forward selection of fixed effects) to systematically evaluate the contributions of demographic, temporal, and environmental predictors across five stages. Each stage builds directly upon the optimal fixed-effects structure of the preceding stage by introducing a new group of predictors. At each stage, we test different drivers encodings and interactions between the new and existing predictors to identify the optimal configuration, thereby reducing researcher bias by avoiding predetermined structural assumptions. The five incremental modelling stages are:

1. **Baseline stage**: Demographic predictors (age and sex).
2. **Seasonal stage**: Builds on (1) and adds temporal harmonics and day length.
3. **Geolocation stage**: Builds on (2) and adds longitude and latitude.
4. **Temperature stage**: Builds on (2) and adds temperature metrics (mean, maximum, and minimum).
5. **Full stage**: Builds on (2) and (3) combining geolocation with residualised temperature.

This data-driven selection process navigates a large search space of over 400 unique configurations by decomposing it into a tractable sequence of 20 models. We apply this framework independently to RHR and HRV, yielding 20 models for RHR (listed in Table 8) and 20 models for HRV (listed in Table 9). Readers may reference these tables throughout the following stage breakdown to trace how individual model selections were performed.

Stage 1 establishes a demographic baseline using age and sex. We test two model options: model 1.1 with a simple linear interaction ($s \times a$) versus model 1.2 with an interaction incorporating quadratic age ($s \times (a + a^2)$), motivated by established literature (Section 1). In Stage 2, we evaluate the optimal representation of seasonality using month of the year alone and testing two candidate variations: first-order month harmonics (model 2.1) and combined first- and second-order month harmonics (model 2.2). Next, both Stage 3 and Stage 4 build upon the Seasonal Model to independently evaluate the contributions of temperature and geolocation. Specifically, Stage 3 evaluates spatial context using nine candidate models. Models 3.1 and 3.2 serve as a baseline and sanity check, testing whether day length alone or combined with its quadratic term can capture spatial and seasonal variations. This allows us to evaluate whether a simple day-length metric outperforms or matches coordinate-based (latitude and longitude) configurations. Models 3.3 and 3.4 expand on this by adding harmonics and testing whether combined temporal and day-length terms help better explain spatial variation. Models 3.5 – 3.8 test combinations of latitude and longitude (linear latitude, latitude plus longitude, linear and quadratic latitude, and latitude plus longitude with quadratic latitude). Model 3.9 combines the optimal spatial structure from the previous four with a seasonal interaction. Stage 4 introduces temperature across four models. Models 4.1 and 4.2 compare mean temperature against minimum and maximum temperatures to determine which carries stronger information. The winning structure serves as the basis for model 4.3, which adds quadratic terms (e.g., $T_{\text{min}} + T_{\text{min}}^2$), and the model 4.4 model, which incorporates seasonal interactions.

Crucially, in the Geolocation (Stage 3) and Temperature (Stage 4) stages, we evaluate models both with and without seasonal interactions between the month and the newly introduced predictors. Rather than assuming the presence of interactions, we explicitly compare configurations containing only independent, additive effects (e.g., Season + Latitude) against those incorporating multiplicative interaction terms (e.g., Season · Latitude) to identify the optimal configuration based on goodness-of-fit. This allows the data to dictate whether geographic or environmental drivers moderate the baseline seasonal wave or act independently of it, while maintaining model parsimony. Finally, in the Stage 5 (Full), we fit three distinct joint configurations to evaluate the relative strength of geolocation and residualised temperature moderation:

- Latitude-Centric Joint (Model 5.1): Seasonality is moderated by latitude according to the winning fixed-effects structure from Stage 3, with residualised temperature added as an additive effect (Season $\cdot \phi + T^{\text{res}}$). The residualised temperature retains the optimal structure identified in Stage 4.
- Temperature-Centric Joint (Model 5.2): Seasonality is moderated by residualised temperature according to the winning fixed-effects structure from Stage 4, with latitude added as an additive effect (Season $\cdot T^{\text{res}} + \phi$). Latitude retains the optimal structure identified in Stage 3.
- Joint Model (Model 5.3): Both latitude and temperature are incorporated using their respective winning interaction structures from Stages 3 and 4 (Season $\cdot \phi$ + Season $\cdot T^{\text{res}}$).

4.3.1. Model fitting and Evaluation

Across all models, parameters were estimated using the `statsmodels` [91] library in Python, facilitating scalable linear mixed-effects (LME) estimation across millions of observations. Model selection was guided by the Bayesian Information Criterion (BIC) to penalise complexity and prevent overfitting. Candidate models were compared using Maximum Likelihood (ML) estimation. Once selected, the winning models of each stage were refitted using Restricted Maximum Likelihood (REML) to obtain unbiased variance components and standard errors – yielding a negligible numerical difference given our large dataset, but is performed here for statistical completeness and standard practice. The refit also accounts for the degrees of freedom lost during fixed-effect estimation, which ML can otherwise

underestimate.

To assess the overall model performance, we additionally report the Akaike Information Criterion (AIC) to further monitor the goodness-of-fit, the Marginal R^2 (variance attributable to fixed effects) and Conditional R^2 (total variance explained by fixed and random effects) for the model fit [92], alongside the Root Mean Square Error (RMSE) for prediction error (evaluated in original units [bpm] for RHR models and log-transformed space for ln(HRV) models). To audit for collinearity arising from high-order interaction terms, we monitored the generalised Variance Inflation Factor (GVIF), ensuring that the final models did not exhibit severe collinearity (defined as an adjusted $GVIF^{1/(2\cdot df)} > 2$) [93]. Finally, the Intraclass Correlation Coefficient (ICC) was calculated to determine the proportion of variance attributed to stable inter-individual differences. The model assumptions of normality and homoscedasticity were verified through visual inspection of Q-Q and residual plots.

Table 8 | **Model Specification for the RHR Incremental LME Framework.** The table illustrates the realised path of the progressive model selection process for Resting Heart Rate (RHR). The framework constructs the candidate models at each stage by building upon the optimal model (determined by BIC) from the preceding stage. Predictors marked with ✓ indicate that the term within a given column is included within the model. Interaction terms are denoted by · in the top row. The path shown here represents the realised selection process for RHR. Models 1.2, 2.2, 3.9, 4.4, and 5.3 emerged as stage winners, highlighted in bold.

		Variables																											
		Demographics					**Seasonal**					**Geolocation**					**Temperature**													
Level	**M**	a	a^2	s	$a \cdot s$	$a^2 \cdot s$	h	d	d^2	$d \cdot h$	$d^2 \cdot h$	ϕ	ϕ^2	λ	$\phi \cdot h$	$\phi^2 \cdot h$	T	T_{max}	T_{max}^2	T_{min}	T_{min}^2	$T_{max} \cdot h$	$T_{max}^2 \cdot h$	$T_{min} \cdot h$	$T_{min}^2 \cdot h$					
1 Baseline	1	✓		✓	✓																								
	2	✓	✓	✓	✓	✓																							
2 Seasonal	1	✓	✓	✓	✓	✓	$\checkmark^{1}$																						
	2	✓	✓	✓	✓	✓	$\checkmark^{1,2}$																						
3 Geolocation	1	✓	✓	✓	✓	✓		✓																					
	2	✓	✓	✓	✓	✓		✓	✓																				
	3	✓	✓	✓	✓	✓	$\checkmark^{1,2}$	✓		$\checkmark^{1,2}$																			
	4	✓	✓	✓	✓	✓	$\checkmark^{1,2}$	✓	✓	$\checkmark^{1,2}$	$\checkmark^{1,2}$																		
	5	✓	✓	✓	✓	✓	$\checkmark^{1,2}$							✓															
	6	✓	✓	✓	✓	✓	$\checkmark^{1,2}$					✓		✓															
	7	✓	✓	✓	✓	✓	$\checkmark^{1,2}$					✓	✓																
	8	✓	✓	✓	✓	✓	$\checkmark^{1,2}$					✓	✓	✓															
	9	✓	✓	✓	✓	✓	$\checkmark^{1,2}$					✓	✓	✓	$\checkmark^{1,2}$	$\checkmark^{1,2}$													
4 Temperature	1	✓	✓	✓	✓	✓	$\checkmark^{1,2}$										✓												
	2	✓	✓	✓	✓	✓	$\checkmark^{1,2}$											✓		✓									
	3	✓	✓	✓	✓	✓	$\checkmark^{1,2}$											✓	✓	✓	✓								
	4	✓	✓	✓	✓	✓	$\checkmark^{1,2}$											✓	✓	✓	✓	$\checkmark^{1,2}$	$\checkmark^{1,2}$	$\checkmark^{1,2}$	$\checkmark^{1,2}$				
5 Full	1	✓	✓	✓	✓	✓	$\checkmark^{1,2}$					✓	✓	✓	$\checkmark^{1,2}$	$\checkmark^{1,2}$		✓	✓	✓	✓								
	2	✓	✓	✓	✓	✓	$\checkmark^{1,2}$					✓	✓	✓				✓	✓	✓	✓	✓	$\checkmark^{1,2}$	$\checkmark^{1,2}$	$\checkmark^{1,2}$				
	3	✓	✓	✓	✓	✓	$\checkmark^{1,2}$					✓	✓	✓	$\checkmark^{1,2}$	$\checkmark^{1,2}$		✓	✓	✓	✓	✓	$\checkmark^{1,2}$	$\checkmark^{1,2}$	$\checkmark^{1,2}$				

Notes: Fixed-effects defined as: a, age; s, sex; d, daylight; ϕ, latitude; λ, longitude terms $\{\lambda_{\sin}, \lambda_{\cos}\}$; T, T_{min}, T_{max}, temperatures. The harmonic term h is indicated by ticks with superscripts denoting the harmonic order: $\checkmark^{1}$ includes first-order terms $\{m_{\sin_1}, m_{\cos_1}\}$; $\checkmark^{1,2}$ includes both fundamental and second harmonic $\{m_{\sin_2}, m_{\cos_2}\}$ harmonics. For Stage 5 (Full) models, temperature variables are residualised against latitude (T^{res}).

Table 9 | **Model Specification for the HRV Incremental LME Framework.** The table illustrates the incremental modelling path for Heart Rate Variability (HRV). The framework constructs the candidate models at each stage by building upon the optimal model (determined by BIC) from the preceding stage. Predictors marked with ✓ indicate that the term within a given column is included within the model. Interaction terms are denoted by · in the top row. The path shown here represents the realised selection process for HRV on the full cohort. Models 1.2, 2.2, 3.9, 4.4, and 5.3 emerged as stage winners, highlighted in bold.

		Variables																						
		Demographics					**Seasonal**					**Geolocation**				**Temperature**								
Level	**M**	a	a^2	s	$a \cdot s$	$a^2 \cdot s$	h	d	d^2	$d \cdot h$	$d^2 \cdot h$	ϕ	ϕ^2	λ	$\phi \cdot h$	T	T_{max}	T^2_{max}	T_{min}	T^2_{min}	$T_{max} \cdot h$	$T^2_{max} \cdot h$	$T_{min} \cdot h$	$T^2_{min} \cdot h$
1 Baseline	1	✓		✓	✓																			
	2	✓	✓	✓	✓	✓																		
2 Seasonal	1	✓	✓	✓	✓	✓	$✓^{1}$																	
	2	✓	✓	✓	✓	✓	$✓^{1,2}$																	
3 Geolocation	1	✓	✓	✓	✓	✓		✓																
	2	✓	✓	✓	✓	✓		✓	✓															
	3	✓	✓	✓	✓	✓	$✓^{1,2}$	✓		$✓^{1,2}$														
	4	✓	✓	✓	✓	✓	$✓^{1,2}$	✓	✓	$✓^{1,2}$	$✓^{1,2}$													
	5	✓	✓	✓	✓	✓	$✓^{1,2}$					✓												
	6	✓	✓	✓	✓	✓	$✓^{1,2}$					✓		✓										
	7	✓	✓	✓	✓	✓	$✓^{1,2}$					✓	✓	✓										
	8	✓	✓	✓	✓	✓	$✓^{1,2}$					✓	✓											
	9	✓	✓	✓	✓	✓	$✓^{1,2}$					✓		✓	$✓^{1,2}$									
4 Temperature	1	✓	✓	✓	✓	✓	$✓^{1,2}$									✓								
	2	✓	✓	✓	✓	✓	$✓^{1,2}$										✓		✓					
	3	✓	✓	✓	✓	✓	$✓^{1,2}$										✓	✓	✓	✓				
	4	✓	✓	✓	✓	✓	$✓^{1,2}$										✓	✓	✓	✓	$✓^{1,2}$	$✓^{1,2}$	$✓^{1,2}$	$✓^{1,2}$
5 Full	1	✓	✓	✓	✓	✓	$✓^{1,2}$					✓		✓	$✓^{1,2}$		✓	✓	✓	✓				
	2	✓	✓	✓	✓	✓	$✓^{1,2}$					✓		✓			✓	✓	✓	✓	✓	$✓^{1,2}$	$✓^{1,2}$	$✓^{1,2}$
	3	✓	✓	✓	✓	✓	$✓^{1,2}$					✓		✓	$✓^{1,2}$		✓	✓	✓	✓	✓	$✓^{1,2}$	$✓^{1,2}$	$✓^{1,2}$

Notes: Fixed-effects defined as: a, age; s, sex; d, daylight; ϕ, latitude; λ, longitude terms $\{\lambda_{\sin}, \lambda_{\cos}\}$; T, T_{min}, T_{max}, temperatures. The harmonic term h is indicated by ticks with superscripts denoting the harmonic order: $✓^{1}$ includes first-order terms $\{m_{\sin_1}, m_{\cos_1}\}$; $✓^{1,2}$ includes both fundamental and second harmonic $\{m_{\sin_2}, m_{\cos_2}\}$ harmonics. For Stage 5 (Full) models, temperature variables are residualised against latitude (T^{res}).

References

[1] Stein, P. K., Kleiger, R. E. & Rottman, J. N. Differing effects of age on heart rate variability in men and women. *The American Journal of Cardiology* **80**, 302–305 (1997).

[2] Pham, T., Lau, Z. J., Chen, S. A. & Makowski, D. Heart rate variability in psychology: A review of HRV indices and an analysis tutorial. *Sensors* **21**, 3998 (2021).

[3] Dyer, A. R. *et al.* Heart rate as a prognostic factor for coronary heart disease and mortality: findings in three Chicago epidemiologic studies. *American Journal of Epidemiology* **112**, 736–749 (1980).

[4] Buchheit, M. & Gindre, C. Cardiac parasympathetic regulation: respective associations with cardiorespiratory fitness and training load. *American Journal of Physiology-Heart and Circulatory Physiology* **291**, H451–H458 (2006).

[5] Cooney, M. T. *et al.* Elevated resting heart rate is an independent risk factor for cardiovascular disease in healthy men and women. *American Heart Journal* **159**, 612–619 (2010).

[6] Saxena, A. *et al.* Protective role of resting heart rate on all-cause and cardiovascular disease mortality. *Mayo Clinic Proceedings* **88**, 1420–1426 (2013).

[7] Jensen, M. T. Resting heart rate and relation to disease and longevity: past, present and future. *Scandinavian Journal of Clinical and Laboratory Investigation* **79**, 108–116 (2019).

[8] Nolan, J. *et al.* Prospective study of heart rate variability and mortality in chronic heart failure: results of the United Kingdom heart failure evaluation and assessment of risk trial (UK-heart). *Circulation* **98**, 1510–1516 (1998).

[9] Kim, H.-G., Cheon, E.-J., Bai, D.-S., Lee, Y. H. & Koo, B.-H. Stress and heart rate variability: a meta-analysis and review of the literature. *Psychiatry Investigation* **15**, 235 (2018).

[10] Kaur, B. *et al.* Heart rate variability (HRV): an indicator of stress. In *Independent Component Analyses, Compressive Sampling, Wavelets, Neural Net, Biosystems, and Nanoengineering XII*, vol. 9118, 177–184 (SPIE, 2014).

[11] Järvelin-Pasanen, S., Sinikallio, S. & Tarvainen, M. P. Heart rate variability and occupational stress—systematic review. *Industrial Health* **56**, 500–511 (2018).

[12] Schiweck, C., Piette, D., Berckmans, D., Claes, S. & Vrieze, E. Heart rate and high frequency heart rate variability during stress as biomarker for clinical depression. A systematic review. *Psychological Medicine* **49**, 200–211 (2019).

[13] Thayer, J. F., Åhs, F., Fredrikson, M., Sollers III, J. J. & Wager, T. D. A meta-analysis of heart rate variability and neuroimaging studies: implications for heart rate variability as a marker of stress and health. *Neuroscience & Biobehavioral Reviews* **36**, 747–756 (2012).

[14] Gonzales, T. I. *et al.* Resting heart rate is a population-level biomarker of cardiorespiratory fitness: The Fenland Study. *PLOS ONE* **18**, e0285272 (2023).

[15] Reimers, A. K., Knapp, G. & Reimers, C.-D. Effects of exercise on the resting heart rate: a systematic review and meta-analysis of interventional studies. *Journal of Clinical Medicine* **7**, 503 (2018).

[16] Althoff, T. Population-scale pervasive health. *IEEE Pervasive Computing* **16**, 75–79 (2017).

[17] Gu, B., Kim, H. S., Kim, H. & Yoo, J.-I. Advancements in Wearable Sensor Technologies for Health Monitoring in Terms of Clinical Applications, Rehabilitation, and Disease Risk Assessment: Systematic Review. *JMIR mHealth and uHealth* **14**, e76084 (2026).

[18] Kurul, F. *et al.* Wearable Sensors for Health Monitoring: Current Applications, Trends, and Future Directions. *Biosensors and Bioelectronics: X* 100727 (2025).

[19] Smarr, B. L. & Schmale, M. S. Digital health and the power of the crowd. *Science Translational Medicine* **12**, eabb6757 (2020).

[20] Quer, G., Radin, J. M. & Steinhubl, S. R. Advancing personalized medicine through everyday wearables. *Nature Medicine* **27**, 938–940 (2021).

[21] Dial, M. B. *et al.* Validation of nocturnal resting heart rate and heart rate variability in consumer wearables. *Physiological Reports* **13**, e70527 (2025).

[22] Higuchi, D., Takahashi, Y., Tanaka, S. & Tomita, Y. Validation of heart rate measured by the consumer-level wearable device Fitbit: a cross-sectional observational study. *Journal of Physical Therapy Science* **37**, 561–566 (2025).

[23] Haghayegh, S., Khoshnevis, S., Smolensky, M. H. & Diller, K. R. Accuracy of PurePulse photoplethysmography technology of Fitbit Charge 2 for assessment of heart rate during sleep. *Chronobiology International* **36**, 927–933 (2019).

[24] Nasr, A. *et al.* Agreement between Fitbit Versa 4 and a reference standard on time-domain nocturnal heart rate variability: A pilot study. *Digital Health* **11**, 20552076251394960 (2025).

[25] Topol, E. J. High-performance medicine: the convergence of human and artificial intelligence. *Nature Medicine* **25**, 44–56 (2019).

[26] Hazra, S. & Bora, K. S. Capitalization of digital healthcare: The cornerstone of emerging medical practices. *Intelligent Pharmacy* (2025).

[27] Narayanswamy, G. *et al.* Towards a General Intelligence and Interface for Wearable Health Data. *arXiv* (2026).

[28] Heydari, A. A. *et al.* The Anatomy of a Personal Health Agent. *arXiv* (2025).

[29] Oura. Introducing Oura Advisor: Your New Personalized AI Coach. https://ouraring.com/blog/oura-advisor/ (2024). Accessed: 8 June 2026.

[30] OpenAI. WHOOP. https://openai.com/index/whoop/ (2023). Accessed: 8 June 2026.

[31] Hughes, A., Shandhi, M. M. H., Master, H., Dunn, J. & Brittain, E. Wearable devices in cardiovascular medicine. *Circulation Research* **132**, 652–670 (2023).

[32] Umetani, K., Singer, D. H., McCraty, R. & Atkinson, M. Twenty-four hour time domain heart rate variability and heart rate: relations to age and gender over nine decades. *Journal of the American College of Cardiology* **31**, 593–601 (1998).

[33] Quer, G., Gouda, P., Galarnyk, M., Topol, E. J. & Steinhubl, S. R. Inter- and intraindividual variability in daily resting heart rate and its associations with age, sex, sleep, BMI, and time of year: Retrospective, longitudinal cohort study of 92,457 adults. *PLOS ONE* **15**, e0227709 (2020).

[34] Raisi-Estabragh, Z. *et al.* Age, sex and disease-specific associations between resting heart rate and cardiovascular mortality in the UK BIOBANK. *PLOS ONE* **15**, e0233898 (2020).

[35] Marks, R. G., Hale, W. E., Moore, M. T., May, F. E. & Stewart, R. B. Resting heart rates in an ambulatory elderly population: an evaluation of age, sex, symptoms, and medication. *Gerontology* **35**, 210–217 (1989).

[36] Moodithaya, S. & Avadhany, S. T. Gender differences in age-related changes in cardiac autonomic nervous function. *Journal of Aging Research* **2012**, 679345 (2012).

[37] Jensen-Urstad, K. *et al.* Heart rate variability in healthy subjects is related to age and gender. *Acta Physiologica Scandinavica* **160**, 235–241 (1997).

[38] Altini, M. & Plews, D. What is behind changes in resting heart rate and heart rate variability? A large-scale analysis of longitudinal measurements acquired in free-living. *Sensors* **21**, 7932 (2021).

[39] Koch, M. *et al.* Assessing the effect of extreme weather on population health using consumer-grade wearables in rural Burkina Faso: observational panel study. *JMIR mHealth and uHealth* **11**, e46980 (2023).

[40] Ong, J. L., Lau, T., Karsikas, M., Kinnunen, H. & Chee, M. W. A longitudinal analysis of COVID-19 lockdown stringency on sleep and resting heart rate measures across 20 countries. *Scientific Reports* **11**, 14413 (2021).

[41] Hernandez, R. *et al.* Resting Heart Rate Variability Measured by Consumer Wearables and Its Associations with Diverse Health Domains in Five Longitudinal Studies. *Sensors* **25**, 7147 (2025).

[42] Medina-Ortiz, D., Castillo-Aguilar, M., Mabe-Castro, D., Mabe-Castro, M. & Nunez, C. Integrated heart rate variability and physiological profiling reveals autonomic phenotypes in older adults from a high-southern-latitude population. *bioRxiv* 2026–03 (2026).

[43] Belisheva, N. K., Martynova, A. A. & Kolomeichuk, S. N. Seasonal variations in the mental state and heart rate variability in adolescents residing beyond the Arctic Circle. *Russian Open Medical Journal* **13**, 416 (2024).

[44] Kristal-Boneh, E., Froom, P., Harari, G., Malik, M. & Ribak, J. Summer-winter differences in 24 h variability of heart rate. *Journal of Cardiovascular Risk* **7**, 141–146 (2000).

[45] Kazuma, N. *et al.* Seasonal variation in heart rate variability in asthmatic children. *Chronobiology International* **17**, 503–511 (2000).

[46] Kristal-Boneh, E., Harari, G. & Green, M. S. Seasonal change in 24-hour blood pressure and heart rate is greater among smokers than nonsmokers. *Hypertension* **30**, 436–441 (1997).

[47] Kristiansen, J., Olsen, A., Skotte, J. H. & Garde, A. H. Reproducibility and seasonal variation of ambulatory short-term heart rate variability in healthy subjects during a self-selected rest period and during sleep. *Scandinavian Journal of Clinical and Laboratory Investigation* **69**, 651–661 (2009).

[48] Koskimäki, H., Kinnunen, H., Rönkä, S. & Smarr, B. Following the heart: what does variation of resting heart rate tell about us as individuals and as a population. In *Adjunct Proceedings of the 2019 ACM International Joint Conference on Pervasive and Ubiquitous Computing and Proceedings of the 2019 ACM International Symposium on Wearable Computers*, 1178–1181 (2019).

[49] Pell, J. & Cobbe, S. Seasonal variations in coronary heart disease. *QJM: An International Journal of Medicine* **92**, 689–696 (1999).

[50] Stewart, S., Keates, A. K., Redfern, A. & McMurray, J. J. Seasonal variations in cardiovascular disease. *Nature Reviews Cardiology* **14**, 654–664 (2017).

[51] Ren, C. *et al.* Ambient temperature, air pollution, and heart rate variability in an aging population. *American Journal of Epidemiology* **173**, 1013–1021 (2011).

[52] Chen, C.-H., Lai, F., Chen, Y.-L. & Guo, Y. L. Effects of Heat Adaptation Behaviors on Resting Heart Rate Response to Summer Temperatures in Older Adults: Wearable Device Panel Study. *JMIR mHealth and uHealth* **13**, e67721 (2025).

[53] Wu, S. *et al.* Temperature, traffic-related air pollution, and heart rate variability in a panel of healthy adults. *Environmental Research* **120**, 82–89 (2013).

[54] O'Connor, F. K. *et al.* Effect of nighttime bedroom temperature on heart rate variability in older adults: an observational study. *BMC Medicine* **23**, 703 (2025).

[55] Alabdulgader, A. *et al.* Long-term study of heart rate variability responses to changes in the solar and geomagnetic environment. *Scientific Reports* **8**, 2663 (2018).

[56] Zenchenko, T. A. & Breus, T. K. The possible effect of space weather factors on various physiological systems of the human organism. *Atmosphere* **12**, 346 (2021).

[57] Vazquez, I. M., Palomino, M. & DelRosso, L. M. Seasonal Variation in Sleep, Respiratory, and Cardiovascular Parameters Assessed by a Wearable Device. *Journal of Biological Rhythms* 07487304261433622 (2026).

[58] Scott, H. *et al.* Variations in sleep duration and timing: Weekday and seasonal variations in sleep are common in an analysis of 73 million nights from an objective sleep tracker. *Sleep* zsaf099 (2025).

[59] Mattingly, S. M. *et al.* The effects of seasons and weather on sleep patterns measured through longitudinal multimodal sensing. *npj Digital Medicine* **4**, 76 (2021).

[60] Li, L., Nakamura, T., Hayano, J. & Yamamoto, Y. Age and gender differences in objective sleep properties using large-scale body acceleration data in a Japanese population. *Scientific Reports* **11**, 9970 (2021).

[61] Liao, J. *et al.* Impact of heat exposure on sleep health and its population vulnerability in the United States. *Environment International* 109942 (2025).

[62] Robbins, R. *et al.* Four-year trends in sleep duration and quality: a longitudinal study using data from a commercially available sleep tracker. *Journal of Medical Internet Research* **22**, e14735 (2020).

[63] Rose, A. H., Schenk, H., Maier, B. F., Brockmann, D. & Winnebeck, E. C. Large-scale wearable data reveal spatiotemporal organization of annual sleep patterns. *bioRxiv* 2025–08 (2025).

[64] Koenig, J. & Thayer, J. F. Sex differences in healthy human heart rate variability: A meta-analysis. *Neuroscience & Biobehavioral Reviews* **64**, 288–310 (2016).

[65] Uusitalo, A. *et al.* Role of genetic and environmental influences on heart rate variability in middle-aged men. *American Journal of Physiology-Heart and Circulatory Physiology* **293**, H1013–H1022 (2007).

[66] Golosheykin, S., Grant, J. D., Novak, O. V., Heath, A. C. & Anokhin, A. P. Genetic influences on heart rate variability. *International Journal of Psychophysiology* **115**, 65–73 (2017).

[67] World Health Organization. *WHO ambient air quality database, 2022 update: status report* (World Health Organization, 2023).

[68] World Health Organization. Global Health Observatory: Prevalence of Obesity among Adults, BMI ≥ 30 (Age-Standardized Estimate). https://www.who.int/data/gho/data/indicators/indicator-details/GHO/prevalence-of-obesity-among-adults-bmi-=-30-(age-standardized-estimate)-(-) (2022). Accessed: 6 August 2026.

[69] Li, Y. *et al.* Short-term association between ambient air pollution and heart rate variability: results from the population-based KORA S4 and FF4 studies. *Particle and Fibre Toxicology* **22**, 26 (2025).

[70] Patten, T. *et al.* The All of Us Research Program's wearables dataset. *Nature Medicine* 1–9 (2026).

[71] Pontin, F., Lomax, N., Clarke, G. & Morris, M. A. Socio-demographic determinants of physical activity and app usage from smartphone data. *Social Science & Medicine* **284**, 114235 (2021).

[72] Bietz, M. J. *et al.* Opportunities and challenges in the use of personal health data for health research. *Journal of the American Medical Informatics Association* **23**, e42–e48 (2016).

[73] Strain, T., Wijndaele, K., Pearce, M. & Brage, S. Considerations for the use of consumer-grade wearables and smartphones in population surveillance of physical activity. *Journal for the Measurement of Physical Behaviour* **5**, 8–14 (2022).

[74] Roggen, D. *et al.* Pixel watch: robust heart rate sensing from multipath PPG and on-device deep learning trained on 10,000 hours of free-living and fitness data. *IEEE Sensors Letters* (2026).

[75] Riley, L. *et al.* The World Health Organization STEPwise approach to noncommunicable disease risk-factor surveillance: methods, challenges, and opportunities. *American Journal of Public Health* **106**, 74–78 (2016).

[76] Lusk, S. L., Hagerty, B. M., Gillespie, B. & Caruso, C. C. Chronic effects of workplace noise on blood pressure and heart rate. *Archives of Environmental Health: An International Journal* **57**, 273–281 (2002).

[77] Kraus, U. *et al.* Individual daytime noise exposure during routine activities and heart rate variability in adults: a repeated measures study. *Environmental Health Perspectives* **121**, 607 (2013).

[78] Rhodes, B. PyEphem: Astronomical Calculations for Python. https://rhodesmill.org/pyephem/ (2011). Accessed: 9 June 2026.

[79] United Nations, Department of Economic and Social Affairs, Population Division. World Population Prospects: The 2024 Revision (Total Population by Sex) [Custom Data]. https://population.un.org/wpp/ (2024). Accessed: 16 April 2026.

[80] Russell, A., Heneghan, C. & Venkatraman, S. Investigation of an estimate of daily resting heart rate using a consumer wearable device. *medRxiv* 19008771 (2019).

[81] National Oceanic and Atmospheric Administration. Global Surface Summary of the Day, GSOD 1.0 [2022]. https://www.ncei.noaa.gov/access/metadata/landing-page/bin/iso?id=gov.noaa.ncdc:C00516 (2022). Accessed: 5 May 2026.

[82] National Oceanic and Atmospheric Administration. NOAA Integrated Surface Database (ISD). https://registry.opendata.aws/noaa-isd/ (2022). Accessed: 5 May 2026.

[83] National Oceanic and Atmospheric Administration. Automated Surface/Weather Observing Systems (ASOS/AWOS). https://www.ncei.noaa.gov/products/land-based-station/automated-surface-weather-observing-systems (2022). Accessed: 5 May 2026.

[84] National Oceanic and Atmospheric Administration. NOAA Global Historical Climatology Network Daily (GHCN-D). https://registry.opendata.aws/noaa-ghcn (2022). Accessed: 5 May 2026.

[85] National Oceanic and Atmospheric Administration. U.S. Climate Reference Network (USCRN). https://www.ncei.noaa.gov/access/crn/ (2022). Accessed: 5 May 2026.

[86] United States Environmental Protection Agency. Air Quality System (AQS) Pre-Generated Data Files: Meteorological Data. https://aqs.epa.gov/aqsweb/airdata/download_files.html (2022). Accessed: 5 May 2026.

[87] Fitbit. Web API. https://dev.fitbit.com/build/reference/web-api/ (2024). Accessed: 1 April 2025.

[88] Gelman, A. Scaling regression inputs by dividing by two standard deviations. *Statistics in Medicine* **27**, 2865–2873 (2008).

[89] Nelson, W. Methods for cosinor-rhythmometry. *Chronobiologia* **6**, 305–323 (1979).

[90] Ferguson, T. *et al.* The Annual Rhythms in Sleep, Sedentary Behavior, and Physical Activity of Australian Adults: A Prospective Cohort Study. *Annals of Behavioral Medicine* **58**, 286–295 (2024).

[91] Seabold, S. & Perktold, J. statsmodels: Econometric and statistical modeling with python. In *9th Python in Science Conference* (2010).

[92] Nakagawa, S. & Schielzeth, H. A general and simple method for obtaining R2 from generalized linear mixed-effects models. *Methods in Ecology and Evolution* **4**, 133–142 (2013).

[93] O'Brien, R. M. A caution regarding rules of thumb for variance inflation factors. *Quality & Quantity* **41**, 673–690 (2007).

Supplementary Files

This is a list of supplementary files associated with this preprint. Click to download.

- seasonalitysupplementarymaterials.pdf